

## Optimal packing of CO at high coverage on Pt(100) and Pt(111) surfaces

Vaidish Sumaria, Luan Nguyen, Franklin Feng Tao, and Philippe Sautet

*ACS Catal.*, **Just Accepted Manuscript** • DOI: 10.1021/acscatal.0c01971 • Publication Date (Web): 17 Jul 2020

Downloaded from [pubs.acs.org](https://pubs.acs.org) on August 3, 2020

### Just Accepted

“Just Accepted” manuscripts have been peer-reviewed and accepted for publication. They are posted online prior to technical editing, formatting for publication and author proofing. The American Chemical Society provides “Just Accepted” as a service to the research community to expedite the dissemination of scientific material as soon as possible after acceptance. “Just Accepted” manuscripts appear in full in PDF format accompanied by an HTML abstract. “Just Accepted” manuscripts have been fully peer reviewed, but should not be considered the official version of record. They are citable by the Digital Object Identifier (DOI®). “Just Accepted” is an optional service offered to authors. Therefore, the “Just Accepted” Web site may not include all articles that will be published in the journal. After a manuscript is technically edited and formatted, it will be removed from the “Just Accepted” Web site and published as an ASAP article. Note that technical editing may introduce minor changes to the manuscript text and/or graphics which could affect content, and all legal disclaimers and ethical guidelines that apply to the journal pertain. ACS cannot be held responsible for errors or consequences arising from the use of information contained in these “Just Accepted” manuscripts.

# Optimal packing of CO at high coverage on Pt(100) and Pt(111) surfaces

Vaidish Sumaria,<sup>†</sup> Luan Nguyen,<sup>‡</sup> Franklin Feng Tao,<sup>‡</sup> and Philippe Sautet<sup>\*,†,¶</sup>

<sup>†</sup>*Department of Chemical and Biomolecular Engineering, University of California, Los Angeles, CA 90094, USA*

<sup>‡</sup>*Department of Chemical and Petroleum Engineering, University of Kansas, Lawrence, Kansas*

<sup>¶</sup>*Department of Chemistry and Biochemistry, University of California, Los Angeles, CA 90094, USA*

E-mail: sautet@ucla.edu

## Abstract

High coverage structures for CO on Pt(111) and Pt(100) surfaces are studied by density functional theory modeling and compared to high pressure scanning tunneling microscopy experiments. Semilocal exchange correlation functionals are known to provide incorrect adsorption site and overestimated adsorption energy for CO on Pt. We develop a simple first-principles correction for the adsorption energy of CO on Pt(111) and Pt(100) using the bond length of adsorbed CO as a descriptor. The energy correction which increases in the order top < bridge < hollow site is used to derive the surface stability diagram for CO adsorbed on 111 and 100 facets of Pt showing the thermodynamically stable CO configurations on the surface as a function of temperature and pressure. High coverage ( $\theta > 0.5$ ) configurations of CO on Pt(111) lead to the formation of superimposed hexagonal/quasi-hexagonal lattice of CO on hexagonal Pt(111) layer from a systematic exploration of such structures. Non-hexagonal structures seen

1  
2  
3 in vacuum and low temperature conditions -  $(\sqrt{3} \times 3)\text{rect-4CO}$  and  $c(\sqrt{3} \times 7)\text{rect-5CO}$   
4 are however only  $5\text{meV}/\text{\AA}^2$  less stable than the hexagonal lattice at similar coverage.  
5 For Pt(100) at  $\theta \geq 0.75$ , the CO molecules adopt a one dimensional coincidence lattice  
6 and we observe the formation of  $(n \times 2)$  unit cells ( $n=4,6,8$ ) with  $(2n-2)$  CO molecules in  
7 each cell on top/quasi-top and bridge/quasi-bridge positions creating a skewed hexag-  
8 onal lattice to reduce CO-CO repulsion with increasing coverage. The computational  
9 results agree with the available experimental observations for Pt(111) and Pt(100).  
10 The integrated theoretical simulation and experimental observation provide structural  
11 data for the study of catalytic reactivity on Pt surfaces in reactions involving high CO  
12 pressures and suggest an approach for understanding the structure of CO molecules on  
13 other metal catalyst surfaces during the catalytic reactions involving high pressure of  
14 CO.  
15  
16  
17  
18  
19  
20  
21  
22  
23  
24  
25  
26  
27

## 28 1 Introduction

29  
30  
31 Adsorption of carbon monoxide on transition metals is frequently regarded as a benchmark  
32 system owing to its importance in CO oxidation<sup>1-4</sup>, water-gas shift reaction<sup>5-8</sup> and Fischer  
33 Tropsch synthesis<sup>9-12</sup> and hence has been a subject of many studies, both experimental and  
34 theoretical. The determination of the CO adsorption site, coverage and assembly structure on  
35 the different transition metal surfaces is a key information for these reactions. It is especially  
36 important to understand the structure and coverage of CO at ambient pressure relevant to  
37 catalytic conditions. Moreover, the simplicity and known adsorption properties of CO, make  
38 it the perfect candidate as a probe molecule in surface science. As a result, adsorption of  
39 CO on platinum surfaces (Pt(100) and Pt(111)) is considered as a model system in the field  
40 and has been studied using wide range of experimental techniques, some of them enabling  
41 to access near ambient to high pressure conditions, including low energy electron diffraction  
42 (LEED), X-ray photoemission spectroscopy (XPS), scanning tunnelling microscopy (STM),  
43 temperature programmed desorption (TPD), calorimetry, work function measurements, Ex-  
44  
45  
46  
47  
48  
49  
50  
51  
52  
53  
54  
55  
56  
57  
58  
59  
60

1  
2  
3 tended X-ray absorption fine structure (EXAFS) etc.<sup>13-34</sup>. CO adsorption on Pt(111) has  
4 been studied both in UHV conditions at low temperature and at atmospheric pressure and  
5 room temperature. Interestingly, different structures are seen. In UHV at low temperature,  
6 CO initially forms a  $(\sqrt{3} \times \sqrt{3})R30^\circ$ -1CO structure at 1/3 ML coverage, occupying the top  
7 site, followed by a well ordered  $c(4 \times 2)$ -2CO (or equivalently  $(\sqrt{3} \times 2)$ rect-2CO) structure at  
8  $\theta=0.5$  ML with equal population of top and bridge sites.<sup>17,18,35,36</sup> The CO arrangement is  
9 not hexagonal in this structure. At higher coverage, a set of compressed, but still non-  
10 hexagonal, structures is found ( $c(\sqrt{3} \times 5)$ rect-3CO,  $\theta=0.6$  ML;  $(\sqrt{3} \times 3)$ rect-4CO,  $\theta=0.67$  ML  
11 ;  $c(\sqrt{3} \times 7)$ rect-5CO,  $\theta=0.71$  ML)<sup>37</sup>. In contrast, at room temperature and atmospheric pres-  
12 sure, STM images show the formation of a hexagonal CO lattice superpositioned on Pt(111)  
13 to construct the so called Moiré pattern structures, for example the  $(\sqrt{19} \times \sqrt{19})R23.4^\circ$ -13CO  
14 commensurate structure at  $\theta=0.68$  ML.<sup>38</sup> The presence of this different set of CO structures  
15 for different conditions is puzzling and the stable or metastable nature of these structures is  
16 unclear until now. On the other hand, the situation for CO adsorption at low coverage on  
17 Pt(100) is somewhat more confused. Bradshaw et al. showed using vibrational spectroscopy  
18 that at 90 K CO occupies the bridge site until 0.5 ML ( $c(2 \times 2)$  structure), while at room  
19 temperature an equal mixture of bridge and top site is seen.<sup>32</sup> Hence the bridge site should  
20 correspond to a slightly lower internal energy. At high coverage, adsorbed CO on Pt(100) is  
21 reported using STM images to adopt a  $c(5\sqrt{2} \times \sqrt{2})R45^\circ$ -3CO unit cell ( $\theta = 0.6$  ML) with 2:1  
22 bridge to top site ratio,<sup>31</sup> followed by a  $(3\sqrt{2} \times \sqrt{2})R45^\circ$ -4CO ( $\theta = 0.67$  ML) unit cell with a  
23 1:1 bridge to top site ratio and a  $c(4 \times 2)$ -3CO unit cell ( $\theta = 0.75$  ML) with 2:1 bridge to top  
24 site adsorption ratio, using LEED.<sup>32</sup> In parallel, synergistic efforts have been applied on the  
25 computational aspects of studying the Pt/CO system.<sup>39-43</sup> A recent work by Gunasooriya  
26 et al. used the vdW-DF non-local functional to model ordered CO structures on Pt(111) at  
27 the high coverage limit.<sup>39</sup>

28  
29  
30  
31  
32  
33  
34  
35  
36  
37  
38  
39  
40  
41  
42  
43  
44  
45  
46  
47  
48  
49  
50  
51  
52  
53 Understanding surface phenomena in heterogeneous catalysis theoretically has been  
54 vastly improved owing to the advancement in density functional theory with the semilo-  
55  
56  
57  
58  
59  
60

cal (GGA) and hybrid exchange correlation (XC) functionals. Despite these successes, a few cases of performing these electronic structure calculations are known to be problematic in determining the correct adsorption site. This challenge is famously known for the Pt(111)/CO system and is coined as “The Pt(111)/CO Puzzle.”<sup>41,44–47</sup>. The widely used semilocal XC functionals - PW91, PBE and RPBE predict chemisorption energies for CO on Pt significantly higher than experimental determination by single crystal calorimetry by approximately 0.37, 0.37 and 0.17 eV respectively.<sup>48,49</sup>. More importantly, all these functionals favour the more coordinated bridge and hollow sites over the top site for Pt(111). On the other hand, more accurate hybrid functionals (PBE0<sup>50</sup>, B3LYP<sup>51</sup>) have been able to predict the correct adsorption site, but provide a CO adsorption energy which is even more overestimated than semilocal functionals, in relation with an overestimated Pt d-band width. Blyholder model<sup>52,53</sup>, describes CO chemisorption on metal surfaces from CO molecular orbitals. This commonly used model suggests interactions of the two CO frontier orbitals, the  $5\sigma$  highest occupied molecular orbital (HOMO) and the  $2\pi^*$  lowest unoccupied molecular orbital (LUMO), with the metal states. The bonding  $5\sigma$  orbital (HOMO) donates electron density to the substrate (known as  $\sigma$ -donation) and the anti-bonding  $2\pi^*$  orbital (LUMO) receives electron density from the the substrate (known as  $2\pi^*$ -backbonding). The extent of backbonding increases with the metallic coordination of the adsorption site (hence is more important for hollow-site) where as the highly directional  $5\sigma$  metal interaction is stronger for the low coordination site, i.e. top site.<sup>54–56</sup> Semilocal XC functionals such as PBE tend to underestimate the HOMO-LUMO gap for CO<sup>41,43,57</sup> and place the unfilled CO  $2\pi^*$  orbital too low in energy which makes it too close in energy to the metal d band, resulting in an unrealistic strengthening of the  $2\pi^* - d$  band bonding interactions (backbonding) which favors multiply bonded sites.

In order to obtain a better agreement with experiments, several studies have developed energy correction schemes to shift the CO LUMO to higher energies, which results in reducing the backbonding and favouring the experimentally observed top site for adsorption. The first

1  
2  
3 method was developed by Kresse et al. where by using potentials with different core radii,  
4 they discovered that there exists a linear relationship linking the difference between top and  
5 hollow site adsorption energies for CO on Pt(111) and the gas-phase energy of the CO  $2\pi^*$   
6 orbital.<sup>41</sup> They developed a GGA+U inspired method to tune the CO  $2\pi^*$  orbital energy and  
7 re-institute the correct top-site for CO adsorption on Pt(111). Following this work, another  
8 method developed by Mason et al. argued the use of GGA+U, since the U parameter is not  
9 known *a priori*.<sup>55</sup> They showed that the CO adsorption energy is not only dependent on the  
10 LUMO level of the free CO molecules but can also be equivalently linearly related to the CO  
11 singlet-triplet excitation energy ( $\Delta E_{S-T}$ ). By extrapolating these linear relationships to the  
12 Configuration Interaction (CI) calculated value of  $\Delta E_{S-T}$ , a correction to the GGA energy  
13 for a respective adsorption site (top, bridge or hollow) was developed. This method was  
14 also shown to be universally working for a variety of metal surfaces.<sup>55</sup> Finally it was shown  
15 that the suggested correction for the adsorption energy also scales with the CO stretching  
16 frequency (which is a function of the adsorption site), which can yield a simpler correction  
17 scheme. This idea was elaborated later by Abild-Pedersen et. al., who suggested that  
18 the adsorption energy correction ( $\Delta$ ) for RPBE XC functional can be simply expressed as  
19  $\Delta = 1.8 - 0.0008 \times \nu_{CO}$ , where  $\nu_{CO}$  is the internal stretch vibration frequency of CO in  $\text{cm}^{-1}$ .<sup>42</sup>  
20 Gajdoš et. al showed that a linear correlation exists between the CO stretching frequency  
21 and C-O bond length which is independent of the coordination of the CO molecule.<sup>43</sup>, which  
22 suggests that a relationship could also exist between the adsorption energy correction and  
23 the C-O bond length.  
24  
25  
26  
27  
28  
29  
30  
31  
32  
33  
34  
35  
36  
37  
38  
39  
40  
41  
42  
43  
44

45 In this work, we first derive this correction scheme for CO adsorption energetics based on  
46 the adsorbed C-O bond length. Similarly to Mason et. al., we consider different pseudopo-  
47 tentials for C and O and re-establish a scaling relation between the adsorption energies at  
48 various sites and the CO gas singlet-triplet excitation energy which is then extrapolated to  
49 the accurate CI value of  $\Delta E_{S-T}$  to find the correction, based on the first principles, needed  
50 to be applied with respect to the GGA energy.<sup>55</sup> We show in addition that this energy  
51  
52  
53  
54  
55  
56  
57  
58  
59  
60

1  
2  
3 correction simply scales with the CO bond length, hence enabling a generalized correction  
4 applicable for low symmetry CO overlayer, where molecules are not in the high symmetry  
5 sites and hence have different CO bond lengths. A generalized correction is developed for  
6 the 111 and 100 facets of platinum. Finally using first principle thermodynamic analysis and  
7 the developed energy corrections, we construct the surface stability diagram that depicts the  
8 stable configurations of CO on the Pt(111) and Pt(100) surfaces as a function of temperature  
9 and CO pressure. We first compare our results to experimental studies in the literature. We  
10 also performed HP-STM experiments on Pt(100) terraces under a high pressure of CO. The  
11 combination between theory and experiments uncovers two high coverage CO structures on  
12 Pt(100), that to our knowledge have not been presented before in the literature. They con-  
13 sist of ( $n \times 2$ ) type unit cells with  $(2n-2)$  CO atoms arranged in a unique pattern with CO on  
14 (quasi) top and (quasi) bridge sites to reduce adsorbate-adsorbate repulsion.  
15  
16  
17  
18  
19  
20  
21  
22  
23  
24  
25  
26  
27  
28

## 29 **2 Methods**

### 30 **2.1 Computational Details**

31  
32  
33 Calculations were performed using the Vienna Ab-initio Simulation Package using the gen-  
34 eral gradient approximation (GGA) Perdew-Burke-Erzenhof (PBE) functional. Two set of  
35 calculations were performed: (i) Developing the correction scheme for CO adsorption on Pt  
36 surfaces, (ii) Using the developed correction scheme to compute the landscape of the ad-  
37 sorbed CO on Pt surfaces at various pressure and temperature conditions. The calculations  
38 for CO adsorption correction scheme are modeled using 1/4 and 1 mono-layer coverage of  
39 adsorbed CO on a six Pt layer slab, separated by 12 Å vacuum from its periodic image in  
40 the z direction. The two bottom layers of the unit cell were kept fixed, and the top four  
41 layers with the adsorbates were allowed to relax with a force criterion of  $<0.01$  eV/Å. A  
42 fermi smearing width of 0.2 eV was applied using the Methfessel-Paxton method (order 2).  
43  
44  
45  
46  
47  
48  
49  
50  
51  
52  
53  
54  
55  
56  
57  
58  
59  
60 A 3x3 surface supercell was considered for Pt(111) and Pt(100) and their Brillouin zones

were sampled using a 7x7x1 k-point mesh. A 0.25 ML and 1 ML coverage was modeled on a 2x2 and 1x1 surface for both Pt(111) and Pt(100) and the k-points were scaled suitably.

The calculation settings used to develop the surface stability diagram are the same as described above. The k-points are suitably scaled for the various unit cells used. We consider the adsorption of CO molecule on various sites with different coverages. The adsorption energy of CO is referenced to gas phase CO and further details of the thermodynamic analysis have been discussed in the supporting information (SI).

The corrections have been obtained using the scheme developed by Mason et al.<sup>55</sup> This involves the following steps: (i) Using various pseudopotentials for C and O listed in Table S1 for  $\theta = 0.25$  ML and Table S2 for  $\theta = 1.00$  ML) we find the scaling relations between the CO adsorption energy on top, fcc and hcp (or hollow) site on Pt(111) (and Pt(100)) and the CO singlet-triplet excitation energy,  $\Delta E_{S-T}$  (SI, Fig. S1 for  $\theta = 0.25$  ML, Fig. S2 for  $\theta = 1.00$  ML) (ii) These scaling relations are then extrapolated to find the adsorption energy at  $\Delta E_{S-T} = 6.095$  eV (excitation energy value reproduced using Coupled-cluster and CI calculations which are comparable with the experimental values.)<sup>58</sup> (iii) The correction is defined as the difference between the extrapolated value of the adsorption energy and the energy obtained using the normal PAW settings for C and O (Details of these results have been included in the SI section S1.1).

To create the surface stability diagram, we systematically select structures manually inspired by an extensive literature review of the available experimental data including hypothetical structures, or proposed variants. Using a number of surface science studies including LEED, STM, EELS, RAIRS, XPS and TPD results we generate a sequence of ordered structures with increasing CO coverage. The symmetry of configurations at low coverage also helps sample various structures manually. For Pt(111) we use a number of different unit cells including p(2x2), p(3x3), p(4x4), p(5x5),  $(\sqrt{3} \times \sqrt{3})R30^\circ$ ,  $(\sqrt{7} \times \sqrt{7})R19.1^\circ$ ,  $(2\sqrt{3} \times 2\sqrt{3})R30^\circ$ ,  $(\sqrt{13} \times \sqrt{13})R14^\circ$ ,  $(\sqrt{19} \times \sqrt{19})R23.4^\circ$ ,  $(\sqrt{21} \times \sqrt{21})R10.8^\circ$ ,  $(3\sqrt{3} \times 3\sqrt{3})R30^\circ$ , c(4x2),  $(\sqrt{3} \times 3)rect$ ,  $c(\sqrt{3} \times 5)rect$ ,  $c(\sqrt{3} \times 7)rect$  with CO adsorbed on multiple of symmetric ( top,



1  
2  
3 bridge, fcc and hcp) and quasi-symmetric sites. Since at high coverage, STM images show  
4 formation of rotated hexagonal CO layers on the Pt(111) surface, we put a special attention  
5 to methodically generate a family of such “Moiré pattern” adsorption structures.<sup>38</sup>. For  
6 Pt(100), at low coverages ( $\theta \leq 0.67$ ), we utilize known experimental results to explore adsorp-  
7 tion of CO on various unit cells including  $c(2 \times 2)$ ,  $c(3 \times 3)$ ,  $c(2\sqrt{2} \times \sqrt{2})R45^\circ$ ,  $c(3\sqrt{2} \times \sqrt{2})R45^\circ$ ,  
8  $c(5\sqrt{2} \times \sqrt{2})R45^\circ$ . At higher coverage ( $\theta \geq 0.75$ ), we show later that CO arranges on an elon-  
9 gated  $c(n \times 2)$  unit cell which helps us explore systematically a number of different coverages  
10 on  $c(n \times 2)$  unit cell with  $n=4,5,6,7,8,9,10$ .

11  
12  
13  
14  
15  
16  
17  
18  
19 The Gibbs free energy for gas-phase CO and for adsorbed CO on the surface is ob-  
20 tained from the DFT energies with ZPE and entropy corrections determined from frequency  
21 calculations performed for all the considered structures using the Harmonic Oscillator ap-  
22 proximation. By displacing the atoms of adsorbate in each direction by a small positive  
23 and negative displacement, we determine six frequencies per CO which includes the typical  
24 CO stretch frequency and five low-frequency modes associated with the Pt-C stretching,  
25 frustrated rotation and translation. Low frequency modes have a large effect on the entropy,  
26 hence we use Truhlar approximation by defining a cutoff frequency of  $100 \text{ cm}^{-1}$  such that all  
27 the frequencies below the cut-off are uniformly shifted up to the cut-off value before entropy  
28 calculation. The configurational entropy does not affect the results for temperatures below  
29 1000 K, hence has been ignored in this analysis. More details of the vibrational calculations  
30 can be found in the SI section S2. All the reported values of adsorption energies have been  
31 corrected using the respective calculated zero point energies.

## 32 33 34 35 36 37 38 39 40 41 42 43 44 45 46 47 **2.2 Experimental Details**

### 48 49 50 **2.2.1 Sample Preparation**

51  
52 Sample preparation was performed in a high pressure scanning tunneling microscope (HP-  
53 STM) system which consists of a HP-STM chamber and sample preparation chamber  
54  
55  
56  
57  
58  
59  
60

1  
2  
3 equipped with a sputter ion gun, mass spectrometer and electron beam heater. The Pt(100)  
4 single crystal (9mm diameter and 1 mm thickness) was purchased from MaTeck GmbH.  
5 Sample cleaning procedure consists of Ar<sup>+</sup> sputtering ( $4 \times 10^{-4}$  Pa Ar at 1000 eV and 10  
6 mA of emission current) at room temperature for 15 minutes, annealing at 800K under O<sub>2</sub>  
7 atmosphere of  $2.7 \times 10^{-6}$  Pa, and annealing at 1200K in UHV for 5 minutes. This procedure  
8 was repeated for 5 to 10 cycles. In the last cycle, an additional reduction step at 800K in  
9  $2.7 \times 10^{-6}$  Pa H<sub>2</sub> was performed. The sample cleanness was checked by STM.  
10  
11  
12  
13  
14  
15  
16  
17

## 18 **2.2.2 High-Pressure Scanning Tunneling Microscope (HP-STM)**

19  
20  
21 Surface structure of Pt(100) under UHV and CO environment (at different pressures) was  
22 studied using a HP-STM system. Details information about this system can be found in the  
23 literature.<sup>59</sup> In short, the sample was placed inside the HP-STM cell (approximately 15mL  
24 in volume) with the cell door remained open for surface checking under UHV environment.  
25 For in-situ experiment, the HP-STM cell door was closed and CO gas was flown through  
26 the cell and over the sample during STM image acquisition. The sample could be heated  
27 simultaneously by an IR laser (810 nm) irradiation on the back of the sample. The sample  
28 temperature was monitored using a K-type thermocouple spot-welded onto the back of the  
29 sample.  
30  
31  
32  
33  
34  
35  
36  
37  
38  
39  
40

# 41 **3 Results and Discussions**

## 42 **3.1 CO adsorption energy correction scheme**

43  
44  
45 Fig. 1 shows the calculated correction for the CO adsorption energy on Pt(111) and Pt(100)  
46 for the top, bridge and hollow site, at a coverage of 0.25 ML. This correction scales with  
47 very small error to the bond length of the adsorbed CO (MAE equal or smaller than 4 meV).  
48 The difference between the correction developed using the two coverages (0.25 and 1 ML)  
49 is small (SI, Fig. S3) and hence we use the relations developed for  $\theta = 0.25$  ML for all our  
50  
51  
52  
53  
54  
55  
56  
57  
58  
59  
60

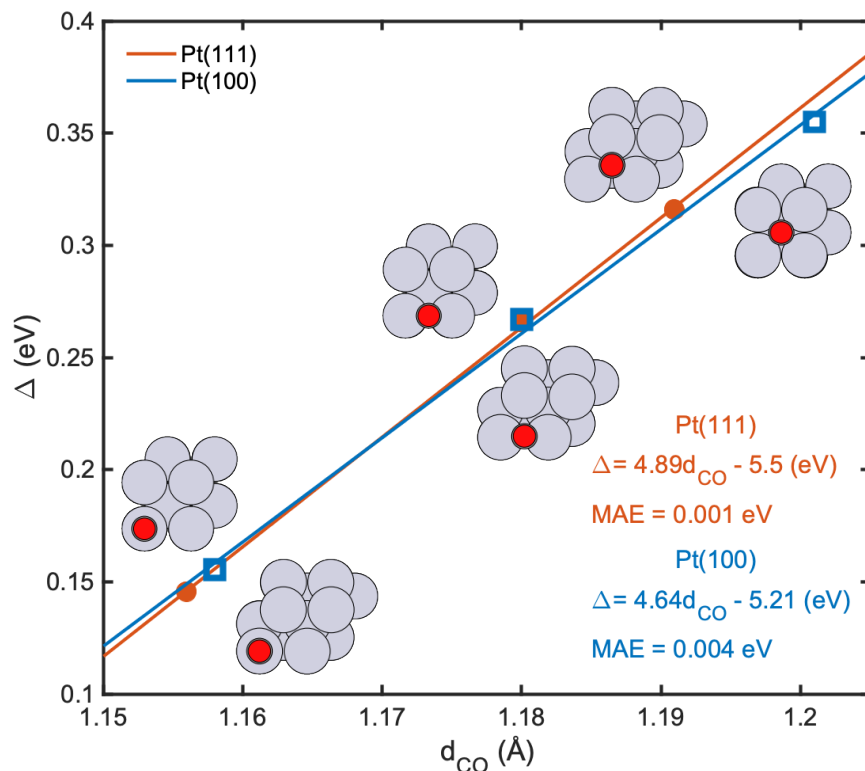


Figure 1: Correction in CO adsorption energy ( $\Delta$ ) plotted against the adsorbed CO bond distance ( $d_{CO}$ ) for various sites (top, bridge and hollow/hcp) for Pt(100) and Pt(111). The corrections are measured by extrapolating the dependence of the adsorption energy ( $E_{CO}^{ad}$ ) on the CO singlet-triplet excitation energy ( $\Delta E_{S-T}$ ) for the various sites on (100) and (111) surfaces of Pt to the coupled cluster and CI calculated value for  $\Delta E_{S-T}$  (refer to SI for more details). CO coverage is 0.25 ML. The red dots ( $\bullet$ ) and the red line represents the data and the correction as a function of CO bond distance for Pt(111) which is given as  $\Delta = 5.13 d_{CO} - 5.83$  where  $d_{CO}$  is in  $\text{\AA}$  and  $\Delta$  in eV. Similarly, the blue squares ( $\square$ ) represent the correction for the Pt(100) surface and can be expressed as  $\Delta = 4.8 d_{CO} - 5.44$ . Both the fits have a mean absolute error (MAE) of smaller than 4 meV per CO. The structures (on Pt(111) and Pt(100)) for which the corresponding correction is calculated are shown.

calculations, irrespective of the coverage. Selecting the relation at 1ML coverage does not change the results presented here.

From previous studies, it has been shown that both  $5\sigma$ -metal d and  $2\pi^*$ -metal d interactions are bonding and the donation from  $5\sigma$  orbital is dominant for CO adsorbed on the top site whereas the back-donation to the  $2\pi^*$  is dominant for the hollow sites.<sup>41,53,60,61</sup> Accordingly the inaccurate DFT-GGA  $\Delta E_{S-T}$  (or the incorrect placement of  $2\pi^*$  orbital) will require the smallest correction for the top site, followed by the bridge and other poly-coordinated

1  
2  
3 sites (threefold hcp/fcc site for Pt(111) and fourfold hollow site for Pt(100)). This explains  
4 the trend we see in the Fig. 1, where the correction required increases with C-O bond dis-  
5 tance which is lowest for top site and highest for hcp/hollow site. Another observation is  
6 that within the range of C-O bond distance plotted in Fig. 1 (1.15-1.25 Å), the correction  
7 calculated at a given value of  $d_{CO}$  is fairly constant between Pt(100) and Pt(111) with a  
8 max difference of 0.015 eV between the two surfaces. This suggests that we can also develop  
9 a general correction scheme that is universal across different facets of Pt which is slightly  
10 more approximate but simpler to use. Nevertheless, in the current work, we proceed with  
11 using the respective corrections for Pt(111) and Pt(100). Table 1 shows a comparison of the  
12 CO adsorption energies obtained experimentally using single crystal adsorption calorimetry  
13 (SCAC) and PBE corrected energies. The predicted energies are lowered in absolute value  
14 by up to 0.3 eV and brought within 0.15 eV error of the experimental values. On Pt(111)  
15 after correction, the adsorption energies of the top, bridge and hollow sites are very similar.  
16 On Pt(100), the bridge site remains 0.1 eV more stable than the top site, and the 4-fold  
17 hollow site is significantly less stable (by 0.57 eV). We will discuss the site dependence of  
18 the energy again below.

19  
20  
21 Table 1: CO adsorption energies (in eV, including the ZPE correction) on Pt(111) and  
22 Pt(100) for top, bridge and hollow adsorption sites as predicted by the PBE exchange correla-  
23 tion functional, after applying the correction to the PBE energies (Corr.) and experimentally  
24 obtained value (Expt.).

Pt(111) (0.25 ML)				Pt(100) (0.25 ML)			
	PBE	Corr.	Expt.		PBE	Corr.	Expt.
Top	-1.58	-1.42	$-1.27 \pm 0.13$ <sup>42,62</sup>	Top	-1.86	-1.70	$-1.57 \pm 0.1$ <sup>29</sup>
Bridge	-1.74	-1.46	-	Bridge	-2.07	-1.80	-
FCC 3-fold Hollow	-1.77	-1.45	-	4-fold Hol- low	-1.60	-1.23	-

### 3.2 Pt(111) surface stability

54 In experimental conditions of heterogeneous catalysis, the structure of the catalytic interface  
55 is far from that in vacuum.<sup>63</sup> Thus to understand the adsorption landscape, we determine

the (T,P) surface stability diagram which covers the surface phases from Ultra High Vacuum and low temperatures to realistic catalytic conditions. Such a thermodynamics based approach in conjunction with ab-initio calculations has been successfully utilized to study Pd hydrogenation catalysts<sup>64</sup>, model RuO<sub>2</sub> structure in O<sub>2</sub> and CO environment<sup>65</sup>, oxygen adsorption on Ag(111)<sup>66</sup>, CO and O<sub>2</sub> induced reconstruction in Pd/Ag(111) surface alloy<sup>67</sup> etc. This method involves comparing the surface stability for systems with varying number of adsorbates. This is achieved by either comparing the unit surface energy or adsorption energy per unit area for the systems. In this work, we use the adsorption energy per unit area since we are more interested in the CO binding energies rather than energies for the overall formation of these surfaces. Since the exact procedure used is similar to that in previous works, we don't discuss it here again, but include the complete analysis in the SI section S2.

Fig. 2 depicts the thermodynamically most stable state of CO on the Pt(111) surface

Table 2: Stable surface structures observed in Fig. 2 (and shown in table 3). The table outlines the types of unit cells, the CO coverage, the average adsorption energy per CO (including  $\Delta ZPE$ ) and the average adsorption Gibbs free energy per CO per unit area of the cell at 300K and 1 atm pressure. Low energy competing metastable structures are also indicated with -a, -b or -c added label

ID	Structure	Coverage	$\Delta E_{CO}^{avg}$ (eV)	$\Delta G_{CO}/A$ (eV/Å <sup>2</sup> )
I	Bare Pt(111) surface	$\theta = 0.00$	-	
II	$(\sqrt{3} \times \sqrt{3})R30^\circ$ -1CO (T)	$\theta = 0.33$	-1.50	-5.03e-02
II-a	$(\sqrt{21} \times \sqrt{21})R10.8^\circ$ -7CO	$\theta = 0.33$	-1.43	-4.64e-02
III	$c(4 \times 2)$ -2CO (2T-2B)	$\theta = 0.50$	-1.39	-6.67e-02
III-a	$(4 \times 2)$ -2CO (3T-1B)	$\theta = 0.50$	-1.34	-6.32e-02
IV	$(2\sqrt{3} \times 2\sqrt{3})R30.0^\circ$ -7CO (3T-3B-1H )	$\theta = 0.583$	-1.34	-7.16e-02
IV-a	$(2\sqrt{3} \times 2\sqrt{3})R30.0^\circ$ -7CO (4T-2B-1H )	$\theta = 0.583$	-1.31	-7.42e-02
IV-b	$(\sqrt{13} \times \sqrt{13})R14.0^\circ$ -7CO	$\theta = 0.54$	-1.36	-7.00e-02
IV-c	$(\sqrt{7} \times \sqrt{7})R19.1^\circ$ -4CO	$\theta = 0.571$	-1.34	-7.24e-02
V	$(\sqrt{19} \times \sqrt{19})R23.4^\circ$ -13CO (1)	$\theta = 0.684$	-1.23	-7.53e-01
V-a	$(\sqrt{19} \times \sqrt{19})R23.4^\circ$ -13CO (2)	$\theta = 0.684$	-1.21	-1.39e-01
V-b	$(\sqrt{3} \times 3)$ rect-4CO	$\theta = 0.677$	-1.23	-7.40e-02
V-c	$c(\sqrt{3} \times 7)$ rect-5CO	$\theta = 0.677$	-1.23	-7.40e-02
VI	$p(2 \times 2)$ -3CO	$\theta = 0.750$	-1.16	-7.47e-02

(lowest adsorption Gibbs energy per unit area) as a function of operational temperature and pressure as predicted after applying the aforementioned correction in the DFT calculated adsorption energies. In total, 61 potential structures were generated (including the bare Pt(111) surface), spanning a coverage between 0 and 1 ML (SI table S3). We put a special attention to systematically generate, among others, all CO adsorption configurations resulting from the matching between an arbitrary (rotated) supercell of Pt(111) and another (rotated) supercell of an hexagonal CO layer, hence generating a family of “Moiré pattern” adsorption structures. Among these 61 structures, 6 are the most stable one in a region of the (T,P) diagram of Fig. 2 and are also presented in table 2. Some structures are very close in energy to these most stable ones. We also include in table 2 the structures which surface free energy is at most  $5 \text{ meV}/\text{\AA}^2$  less stable than the most stable one found in any point of the diagram. Due to inaccuracies in the calculations, it is indeed not possible to exclude that these structures could be found experimentally stable. As expected, with the increase in the chemical potential of CO ( $\sim -2.7 \text{ eV}$  at 600K and  $10^{-6} \text{ Pa}$ , to  $\sim 0 \text{ eV}$  at 100K and  $10^8 \text{ Pa}$ ), we see that the coverage of CO on Pt(111) increases. An interesting feature of the stable structures emerging from our results is that CO tends to form a quasi-hexagonal structure on the Pt(111) surface at high coverages. These hexagonal CO patterns either match the Pt hexagonal orientation on the (111) surface or are rotated at an angle to create a so called family of “Moiré patterns”.

At low pressure and high temperature conditions we find that it is thermodynamically not favorable to have CO adsorbed on the surface (bottom right corner of Fig. 2). With increasing pressure and decreasing temperature, CO first arranges on a  $(\sqrt{3} \times \sqrt{3}) R30^\circ$  unit cell with CO only on the top site (structure (II) in Table 3). The very small preference in the internal energy for the bridge site (Table 2) is counterbalanced by a larger vibrational entropy at the top site, resulting in a most stable top site. This matches the experimentally observed structure first seen in UHV conditions upon dosing CO at a  $1/3 \text{ ML}$  ( $\theta = 0.33$ ) coverage.<sup>17</sup> At 300 K, for  $-1.43 < \Delta\mu_{CO}(T, P) < -1.08 \text{ eV}$ , the  $(\sqrt{21} \times \sqrt{21})R10.8^\circ$ -7CO

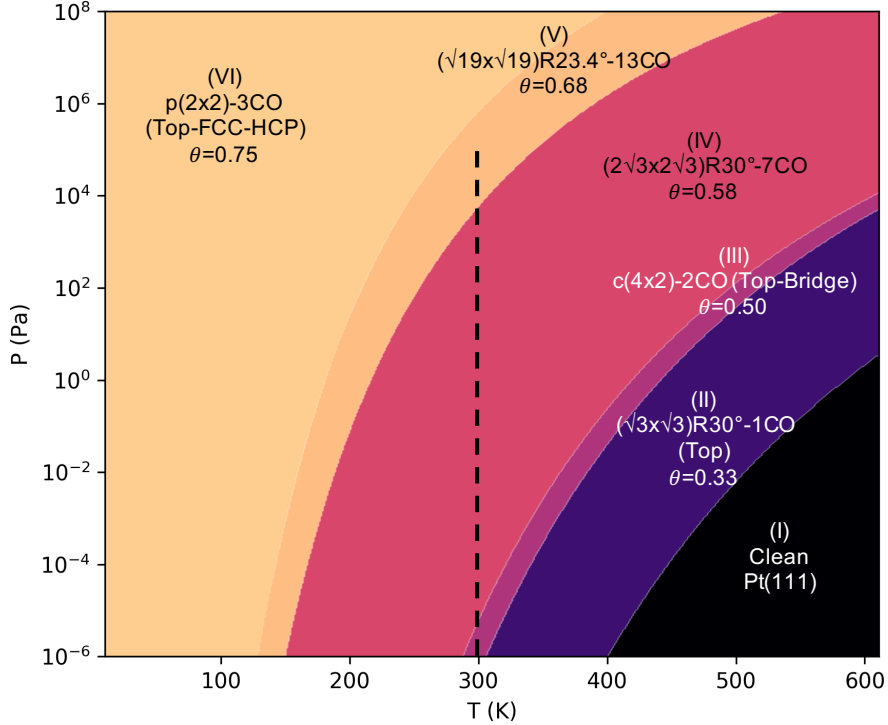


Figure 2: Thermodynamic surface stability diagram depicting the most stable CO coverage as a function of temperature and pressure on Pt(111). The various colors represent the calculated most stable surface terminations as labelled in the figure and shown in table 2. The black dashed line represents the pressure range studied using STM at 300 K by Longwitz et. al. where the superposition of quasi-hexagonal (and hexagonal) lattice of CO on the hexagonal lattice of Pt(111) appears in range of coverage from 0.5 to 0.68 ML.

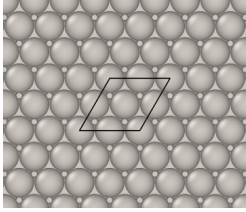
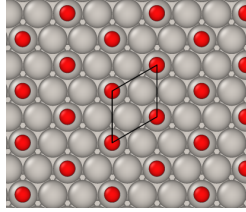
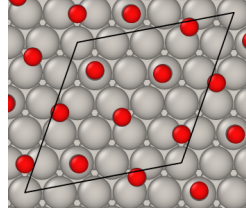
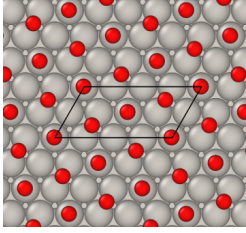
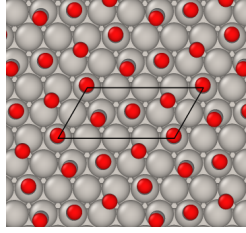
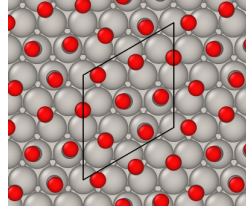
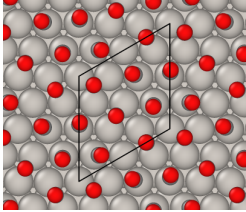
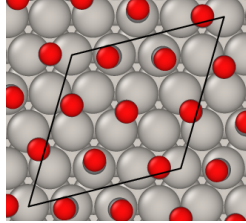
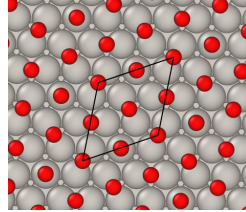
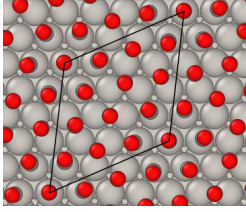
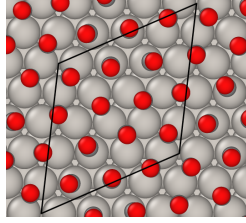
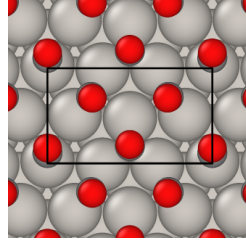
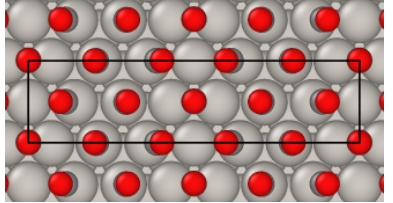
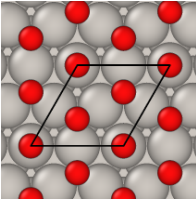
structure ((II-a) in Table 3) is only 4 meV/Å<sup>2</sup> less stable than the ( $\sqrt{3} \times \sqrt{3}$ ) R30° structure. On ( $\sqrt{21} \times \sqrt{21}$ )R10.8°-7CO unit cell, CO arranges on a combination of top and bridge site to form a hexagonal pattern. Further increase in the pressure and decrease in temperature results in half-monolayer coverage with c(4x2)-2CO unit cell that consists of equal population of top and bridge sites (structure (III) in Table 3) which agrees with the experimental studies using LEED, EELS and STM.<sup>18,68-70</sup> At this same coverage at 300 K, for a small range of chemical potential of CO ( $-1.08 < \Delta\mu_{CO}(T, P) < -1.01$  eV), a metastable c(4x2)-2CO structure with 3 CO on top (and quasi top) site and one CO on bridge site (structure (III-a) in Table 3) is found 3.5 meV/Å<sup>2</sup> higher in energy. The CO layer in this stable mixed top-bridge structure is strongly deviating from an hexagonal arrangement. One CO molecule is surrounded by 6 other CO molecules, but the structure is markedly distorted with neighbors

1  
2  
3 at a  $\sqrt{3}$  separation (4.881 Å) and others at  $\sqrt{7}/2$  (3.727 Å). This is the last structure of this  
4 type on the diagram of figure 2 and all other structures found stable at higher coverage will  
5 all be (quasi) hexagonal.  
6  
7

8  
9 The next domain corresponds to structure IV and enters the conditions studied by Long-  
10 witz et al.<sup>38</sup> using STM at room temperature. We will hence follow the dotted black line on  
11 Fig. 2. Along this line (at 300 K), in the pressure range  $10^{-5}$  to  $6 \times 10^3$  Pa, corresponding  
12 to  $-1.01 \lesssim \Delta\mu_{CO}(T, P) \lesssim -0.47$ , we find the  $(2\sqrt{3} \times 2\sqrt{3})R30^\circ$ -7CO structure as most stable  
13 (structure (IV) in table 3). On this unit cell CO molecules occupy 3 (quasi) top, 3 bridge and  
14 1 HCP site forming a quasi-hexagonal arrangement. On the same unit cell, another structure  
15 with CO occupying 4 (quasi)top, 2 bridge and 1 HCP site (structure IV-a in table 3) is only  
16 0.5 meV/Å<sup>2</sup> less stable than the former structure, thus quasi-isoenergetic. STM images show  
17 in this pressure range a Moiré pattern image corresponding to a superstructure rotated by  
18 30° with respect to the Pt lattice, in good agreement with our theoretical geometry, but with  
19 a lattice vector length increasing continuously from 3.2 to 4 times the Pt-Pt distance and  
20 CO coverage from 0.56 to 0.65 ML, explained by the incommensurate nature of the imaged  
21 structure, instead of constant values of 3.46 Å and 0.58 ML in our case. The CO dense row  
22 are rotated by 10-15° with respect to Pt rows, which agree well with our 11.63° value. Our  
23 computed structure can hence be viewed as a (necessarily) commensurate approximate of  
24 an otherwise incommensurate phase evolving with pressure. In this chemical potential range  
25 ( $-1.01 \lesssim \Delta\mu_{CO}(T, P) \lesssim -0.47$ ), we also see some slightly less stable structures with coverages  
26 between 0.5 ML and 0.58 ML. At  $\theta = 0.54$ , the  $(\sqrt{13} \times \sqrt{13})R14^\circ$ -7CO structure ((IV-b) in  
27 Table 3) is at most 9.5 meVÅ<sup>2</sup> less stable, at  $\theta = 0.57$ , the  $(\sqrt{7} \times \sqrt{7})R19.1^\circ$ -4CO structure  
28 ((IV-c) in Table 3) is at most 2 meV/Å<sup>2</sup> less stable compared to the predicted structure at  
29 0.58 ML. These low energy metastable structures have not been seen experimentally, to our  
30 knowledge. At a pressure above  $6 \times 10^3$  Pa, the overlayer switches to another higher coverage  
31 superposition structure  $(\sqrt{19} \times \sqrt{19})R23.4^\circ$ -13CO ((V) in Table 3), with coverage of  $\theta = 0.684$   
32 (13 CO on a 19 surface Pt atoms), which remains stable until  $6 \times 10^5$  Pa, , corresponding to  
33  
34  
35  
36  
37  
38  
39  
40  
41  
42  
43  
44  
45  
46  
47  
48  
49  
50  
51  
52  
53  
54  
55  
56  
57  
58  
59  
60



Table 3: Low energy structures for CO on Pt(111) for various coverages. This includes stable structures found in the surface stability diagram of Fig. 2 (using the same numeric ID) and low energy metastable structures with surface energy at most  $5 \text{ meV}/\text{\AA}^2$  less stable (indicated with the added -a and -b labels).

<p>(I) Clean</p> 	<p>(II) <math>(\sqrt{3} \times \sqrt{3})R30^\circ</math>-1CO (T)</p> 	<p>(II-a) <math>(\sqrt{21} \times \sqrt{21})R10.8^\circ</math>-7CO</p> 
<p>(III) <math>c(4 \times 2)</math>-2CO (2T-2B)</p> 	<p>(III-a) <math>c(4 \times 2)</math>-2CO (3T-1B)</p> 	<p>(IV) <math>(2\sqrt{3} \times 2\sqrt{3})R30.0^\circ</math>-7CO (3T-3B-1H)</p> 
<p>(IV-a) <math>(2\sqrt{3} \times 2\sqrt{3})R30.0^\circ</math>-7CO (4T-2B-1H)</p> 	<p>(IV-b) <math>(\sqrt{13} \times \sqrt{13})R14.0^\circ</math>-7CO</p> 	<p>(IV-c) <math>(\sqrt{7} \times \sqrt{7})R19.1^\circ</math>-4CO</p> 
<p>(V) <math>(\sqrt{19} \times \sqrt{19})R23.4^\circ</math>-13CO</p> 	<p>(V-a) <math>(\sqrt{19} \times \sqrt{19})R23.4^\circ</math>-13CO</p> 	<p>(V-b) <math>(\sqrt{3} \times 3)</math>rect-4CO (1T-3B)</p> 
<p>(V-c) <math>c(\sqrt{3} \times 7)</math>rect-5CO</p> 	<p>(VI) <math>p(2 \times 2)</math>-3CO</p> 	

1  
2  
3 the CO chemical potential interval of  $-0.47 \lesssim \Delta\mu_{CO}(T, P) \lesssim -0.34$ . The coincidence lattice  
4 places the CO adsorbate on various adsorption sites ((quasi)top, bridge, fcc, hcp), but 7 of  
5 the 13 CO molecules are on the top or quasi-top sites. This commensurate structure is clearly  
6 seen in the STM experiment at RT and  $9.6 \times 10^4$  Pa.<sup>38</sup> The simulated STM image (SI fig. S6)  
7 of this structure also compares well with the experiment. As shown earlier by Bocquet et  
8 al. in the case of low coverage CO, the bright spot on the image corresponds to CO on the  
9 top/quasi-top site and the lesser bright spot corresponds to the bridge/quasi-bridge/hollow  
10 site.<sup>40</sup> On the same unit cell, another orientation of CO with 5 of the 13 CO on the top or  
11 quasi-top sites ((V-a) in Table 3) is observed to be slightly less stable with an energy dif-  
12 ference of only  $1.4 \text{ meV}/\text{\AA}^2$ . Starting from the previously described incommensurate Moiré  
13 pattern rotated by  $30^\circ$  (at  $\theta=0.5$ ), the experimental structure undergoes a rotational phase  
14 transition at  $\theta \sim 0.6$ - $0.65$  ML, with a decrease of the superstructure angle with respect to the  
15 Pt lattice from  $30^\circ$  to  $23.4^\circ$  and the stabilization of the lattice vector length at 4.36 times the  
16 Pt-Pt distance. This is in very good agreement with the calculated structural parameters  
17 for the  $(2\sqrt{3} \times 2\sqrt{3})R30^\circ$ -7CO and  $(\sqrt{19} \times \sqrt{19})R23.4^\circ$ -13CO coincidence lattices. Hence,  
18 for coverage above 0.5 ML, structures calculated to be most stable correspond to the quasi-  
19 hexagonal ones seen by the room temperature atmospheric pressure experiments. Let us  
20 now compare with the non-hexagonal structures found in UHV and high pressure.

21  
22  
23  
24  
25  
26  
27  
28  
29  
30  
31  
32  
33  
34  
35  
36  
37  
38  
39 At a coverage of 0.6, three different models have been proposed for a  $c(\sqrt{3} \times 5)$ rect-  
40 3CO unit cell with bridge:top occupation ratio of 2:1 (proposed by Petrova and Yakovkin<sup>71</sup>,  
41 shown in SI table S3 ID: 38) and 1:2 (proposed by Persson et al.<sup>37</sup> and Avery et al.<sup>13</sup> having  
42 different CO relative positions, shown in SI table S3 ID: 39,40 respectively). Structures 39  
43 and 40 are found to be quasi-isoenergetic and more stable than 38. Gunasooriya et. al  
44 using computational thermodynamics shows that the structures with a bridge:top ratio of  
45 1:2 are stable.<sup>39</sup> However, our calculations show that the  $(\sqrt{19} \times \sqrt{19})R23.4^\circ$ -13CO overlayer  
46 is significantly more stable (with an energy difference of  $16.8 \text{ meV}/\text{\AA}^2$  at 300K) compared  
47 to the  $c(\sqrt{3} \times 5)$ -3CO structure, and the later is thus not visible in the surface stability  
48  
49  
50  
51  
52  
53  
54  
55  
56  
57  
58  
59  
60

1  
2  
3 diagram. Similarly, at a coverage of 0.67, on the basis of LEED and HREELS studies,  
4 Avery<sup>13</sup> suggested the formation of a  $(\sqrt{3} \times 3)$ rect-4CO type unit cell with 1:3 bridge:top  
5 site occupation (shown in table 3 V-b). On the same unit cell, Biberian and van Hove<sup>20</sup>  
6 showed a 3:1 bridge:top occupation using LEED and TPD studies (SI, table S3, structure  
7 50). Our results find the Avery structure slightly more stable than that of Biberian and  
8 van Hove, in agreement with the calculations by Gunasooriya et. al. On comparing the  
9  $(\sqrt{19} \times \sqrt{19})R23.4^\circ$ -13CO with the  $(\sqrt{3} \times 3)$ rect-4CO structure, we find the former structure  
10 is numerically more stable but only by a small energy difference of 3 meV/Å<sup>2</sup>.<sup>39</sup> At a higher  
11 coverage of 0.714 ML, Persson et. al showed LEED studies that suggest a  $c(\sqrt{3} \times 7)$ rect-  
12 5CO (shown in table 3 V-c).<sup>37</sup> Comparing this structure with the  $(\sqrt{19} \times \sqrt{19})R23.4^\circ$ -13CO  
13 structure shows that the latter is only 2.4 meV/Å<sup>2</sup> (maximum) more stable. Hence, CO on  
14 Pt(111) at high coverage can present two types of structures (hexagonal and non hexagonal)  
15 with very similar stability. Our calculation find the hexagonal Moiré pattern type structures  
16 to be more stable, but non-hexagonal structures (as  $(\sqrt{3} \times 3)$ rect-4CO and  $c(\sqrt{3} \times 7)$ rect-5CO)  
17 come very close in energy, quasi degenerate. This explains the fact that these two types of  
18 structures can be found in different experimental conditions.

19  
20  
21  
22  
23  
24  
25  
26  
27  
28  
29  
30  
31  
32  
33  
34  
35 At low temperatures and very high  $\mu_{CO}(T, P) \gtrsim -0.34$  (at 300K), we find a (2x2) struc-  
36 ture with 3 CO molecules on a top, an fcc and an hcp hollow site. Such a structure, has  
37 been reported in aqueous acidic medium for Pt(111) using STM along with IRAS<sup>72</sup> and for  
38 Pd(111) using computational results as well as RAIRS/HREELS spectra.<sup>73</sup> From all the  
39 considered coverages of CO, we find that the adsorption saturates at this coverage of 0.75  
40 ML. Comparing this structure with  $c(\sqrt{3} \times 7)$ rect-5CO (0.714 ML), in the chemical potential  
41 range ( $\mu_{CO}(T, P) \gtrsim -0.34$  (at 300K)) where the former is stable, we find that 0.75 ML struc-  
42 ture is only 4.8 meV/Å<sup>2</sup> (maximum) more stable. This once again reinforces the possible  
43 presence of quasi degenerate hexagonal and non-hexagonal packing of CO at high coverages  
44 on Pt(111).  
45  
46  
47  
48  
49  
50  
51  
52  
53  
54

55 The effect the developed correction scheme has a marked effect on the stability diagram  
56  
57  
58  
59  
60

1  
2  
3 of Pt(111). The stability diagram without the the suggested correction has a very different  
4 appearance (supporting information fig. S8). Low coverage phases appear before 1/3 ML,  
5 and the fcc hollow site is the preferred site over the experimentally observed top site. Without  
6 the applied corrections, the  $c(4 \times 2)$  0.5 ML coverage domain does not appear, which also  
7 disagrees with the experimental findings. At  $\theta = 0.58$ , the  $(2\sqrt{3} \times 2\sqrt{3})R30^\circ$ -7CO Moiré  
8 pattern is predicted but for a much smaller range of temperature and pressure; and the  
9  $(\sqrt{19} \times \sqrt{19})R23.4^\circ$ -13CO structure at  $\theta = 0.68$  is not seen, at the benefit on a strongly  
10 extended domain for the high coverage  $p(2 \times 2)$  (0.75 ML), which appears at 300 K for a  
11 pressure of CO 8 orders of magnitude lower than when including the correction. Hence  
12 application of the correction has a major qualitative effect on the predicted stability diagram  
13 and markedly improves the agreement with experimental results. Using the generalized  
14 correction,  $\Delta = 4.77d_{CO} - 5.37$  eV, valid for both Pt(111) and Pt(100), results in the same  
15 stability diagram, showing that a single surface independent correction appears sufficient.  
16  
17  
18  
19  
20  
21  
22  
23  
24  
25  
26  
27  
28  
29  
30

### 3.3 Pt(100) surface stability

31  
32  
33 Fig. 3 depicts the most thermodynamically stable state of the CO on Pt(100) surface as  
34 a function of temperature and CO pressure, while adsorption energies and geometries are  
35 provided in table 4 and 5 respectively. 29 structures have been generated in total (including  
36 the bare Pt(100) surface), and 12 appear on the stability diagram (SI table S4). For high  
37 temperature and low pressure the clean surface is the most stable (bottom right corner of Fig.  
38 3). Increasing the chemical potential  $\Delta\mu_{CO}(T, P)$  (reducing the temperature or increasing  
39 the pressure), we find two narrow stable domains corresponding to low coverage adsorption  
40 of CO at 0.11 and 0.25 ML. CO is calculated to adsorb slightly more favorably on the bridge  
41 site. The first wide domain of stability corresponds to the  $c(2 \times 2)$ -1CO structure ( $\theta=0.5$   
42 ML) with both CO on bridge sites. The difference in energy between CO on top vs CO on  
43 bridge site (structure IV and IV-a in table 4) is again small 2.5 meV/Å<sup>2</sup>. IRAS experiments  
44 for low coverage CO adsorption (until 0.5 ML) on Pt(100) at 90 K gives rise to a single  
45  
46  
47  
48  
49  
50  
51  
52  
53  
54  
55  
56  
57  
58  
59  
60

band at  $1874\text{ cm}^{-1}$ , assigned to bridge bonded CO, in good agreement with the calculated frequency of  $1863\text{ cm}^{-1}$ .<sup>32</sup> A band at  $2075\text{ cm}^{-1}$ , assigned to top site CO, only appears at higher exposure. Low coverage adsorption at 300 K gives rise to two bands, one at  $2067\text{ cm}^{-1}$ , for top site, and another at  $1870\text{ cm}^{-1}$ , for bridge-site CO. From these experiments, Martin et al. concluded that the ratio of bridge to linear site occupancy at low coverages is temperature-dependent with a favored  $c(2\times 2)$  (or equivalently  $(\sqrt{2} \times \sqrt{2})R45^\circ$ )  $0.5\text{ ML}$  structure with bridge sites at low temperature, and a superposition of bridge site and top sites domains at high temperature.<sup>32</sup> This agrees with a slightly more stable energy for bridge site at low coverage. For this  $0.5\text{ ML}$  coverage, a  $(2\sqrt{2} \times \sqrt{2})$  unit cell can provide a different arrangement of bridge sites which is almost degenerate (IVb in table 5). A  $p(2\times 2)$ -2CO unit cell with equal population of top and bridge site (SI table S4 structure 11) is also compared with the symmetric  $c(2\times 2)$ -1CO structures, and the former structure is found only  $4\text{ meV}/\text{\AA}^2$  less stable.

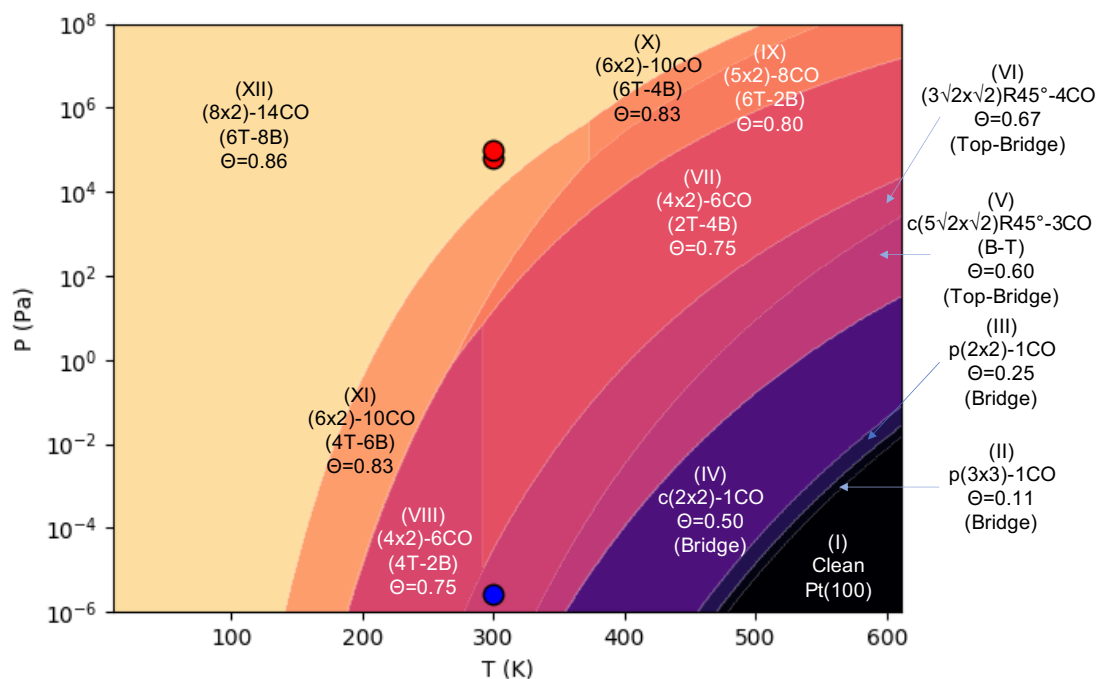


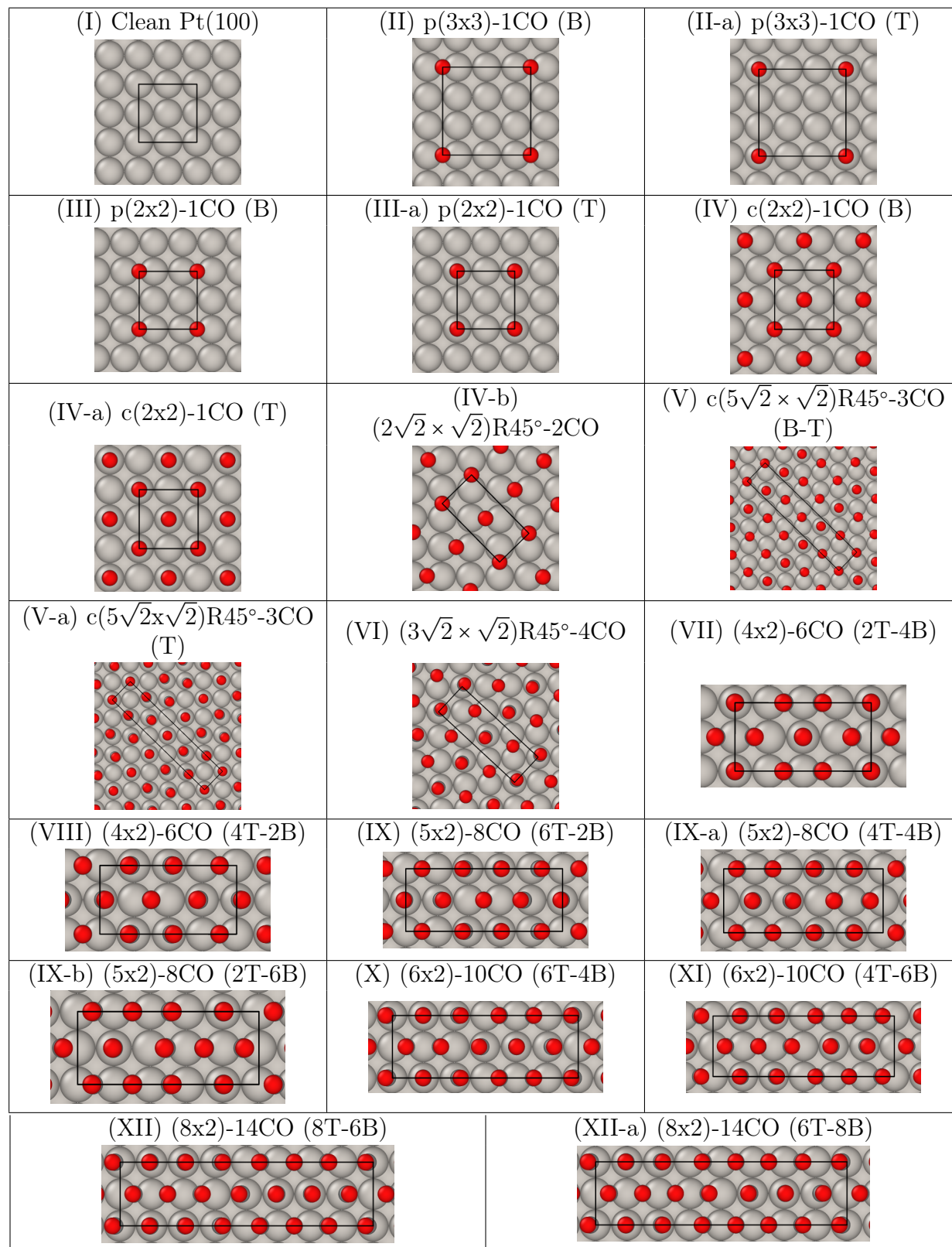
Figure 3: Thermodynamic surface stability diagram depicting the most stable CO coverage as a function of the temperature and pressure on Pt(100). Above  $\theta \geq 0.75$ , we see formation of the  $c(n\times 2)$  unit cells with  $(n-2)\text{CO}$  ( $n=4,6,8$ ) which are observed in STM images discussed in the paper. The red and blue dots on the plot represent the different pressures at room temperature where HP-STM images were obtained.

Table 4: Stable surface structures observed in Fig. 3 (and shown in table 5). The table outlines the types of unit cells, the CO coverage, the average adsorption energy per CO (including  $\Delta ZPE$ ) and the average adsorption Gibbs free energy per CO per unit area of the cell at 300K and 1 atm pressure. Low energy metastable structures are also (indicated with -a or -b added label).

ID	Unit Cell	Coverage	$\Delta E_{CO}^{avg}$ (eV)	$\Delta G_{CO}/A$ (eV/Å <sup>2</sup> )
I	Bare Pt(100) surface	$\theta = 0.00$	-	-
II	p(3×3)-1CO (B)	$\theta = 0.11$	-1.82	-0.019
II-a	p(3×3)-1CO (T)	$\theta = 0.11$	-1.71	-0.018
III	p(2×2)-1CO (B)	$\theta = 0.25$	-1.80	-0.042
III-a	p(2×2)-1CO (T)	$\theta = 0.25$	-1.70	-0.039
IV	c(2×2)-1CO (B)	$\theta = 0.50$	-1.76	-0.081
IV-a	c(2×2)-1CO (T)	$\theta = 0.50$	-1.71	-0.078
IV-b	(2√2 × √2)R45°-2CO (B)	$\theta = 0.50$	-1.75	-0.081
V	c(5√2 × √2)R45°-3CO (B-T)	$\theta = 0.60$	-1.68	-0.092
V-a	c(5√2 × √2)R45°-3CO (T)	$\theta = 0.60$	-1.61	-0.086
VI	(3√2 × √2)R45°-4CO	$\theta = 0.67$	-1.64	-0.098
VII	(4×2)-6CO (2T-4B)	$\theta = 0.75$	-1.58	-0.104
VIII	(4×2)-6CO (4T-2B)	$\theta = 0.75$	-1.57	-0.104
IX	(5×2)-8CO (6T-2B)	$\theta = 0.8$	-1.52	-0.106
IX-a	(5×2)-8CO (4T-4B)	$\theta = 0.8$	-1.51	-0.105
IX-b	(5×2)-8CO (2T-6B)	$\theta = 0.8$	-1.50	-0.103
X	(6×2)-10CO (6T-4B)	$\theta = 0.83$	-1.49	-0.106
XI	(6×2)-10CO (4T-6B)	$\theta = 0.83$	-1.48	-0.106
XII	(8×2)-14CO (6T-8B)	$\theta = 0.875$	-1.44	-0.107
XII-a	(8×2)-14CO (8T-6B)	$\theta = 0.875$	-1.44	-0.106

The next stable surface on the diagram (Figure 3) we find is the c(5√2 × √2)R45°-3CO unit cell with  $\theta=0.6$  ML. On this unit cell, we compare two different CO adsorption: (i) 4 CO on bridge site and 2 on Top and (ii) all 6 CO on the top site ((V) and (V-a) in Table 5). When compared at 300 K, the former structure is only 6 meV/Å<sup>2</sup> more stable than the latter corresponding to an overall average adsorption energy difference on 0.07 eV/CO. STM images and LEED analysis confirm the formation of this c(5√2 × √2)R45°-3CO unit cell with a 2:1 bridge to top ratio of CO occupation.<sup>31,32</sup> On increasing the chemical potential further, CO coverage increases to 0.67 ML on a (3√2 × √2)R45° unit cell with equal ratio of CO on bridge and top sites. This agrees with the experimental analysis from LEED.<sup>32,74</sup>

Table 5: Low energy structures for CO on Pt(100) for various coverages. This includes stable structures in the surface stability diagram of Fig. 2 (using the same numeric ID) and low energy metastable structures with surface energy at most  $5 \text{ meV}/\text{\AA}^2$  less stable (indicated with the added -a and -b labels)



1  
2  
3 For  $\theta \geq 0.75$ , a specific structural pattern was seen for the formation of a dense layer of  
4 CO on Pt(100): the registry of a deformed quasi hexagonal CO layer on the Pt(100) surface.  
5 We observed the formation of elongated  $(n \times 2)$  unit cells with  $[(n \times 2) - 2]$  CO adsorbed  
6 on a combination of top, quasi-top and bridge sites in Fig. 4. Some structures are centered  
7  $(c(n \times 2))$  but for simplicity in the presentation, we will call all of them  $(n \times 2)$ . At  $\theta = 0.75$   
8 a  $(4 \times 2)$ -6CO unit cell with 6 CO is observed to be stable. Two different configurations of  
9 CO on the surface are observed - (i) 2 CO on top, 4 CO on quasi-bridge site (ii) 4 CO on  
10 quasi-top, 2 CO on bridge site (structures VII and VIII shown in table 5). The former is  
11 stable at low pressures below 300 K and the later is stable at higher pressures above 300 K.  
12 Such an arrangement of CO molecules on the surface results from a compromise between the  
13 CO-surface interaction and the repulsive lateral interactions between the CO molecules. It  
14 can be seen that any two CO molecules on the short direction of the unit cell are on different  
15 sites (bridge or top), which allows for a reduced repulsion of the adsorbates. In addition,  
16 this over-layer CO structure was confirmed by in-situ HP-STM result as seen in Fig. 4(a).  
17 Gaseous CO was introduced into the HP-STM cell and maintained at  $2.7 \times 10^{-6}$  Pa ( $2.7 \times 10^{-8}$   
18 mbar) during image acquisition. At this condition, STM image of Pt(100) shows formation  
19 of a domain of  $(4 \times 2)$ -6CO over-layer structure, in conditions which are at the border of the  
20 calculated region of the phase diagram (red dot in Fig. 3). Red circles in Fig. 4(a) indicate  
21 the location of adsorbed CO molecules. The structure present some imperfect order but the  
22 assignment is supported by the average CO-CO distance of the CO over-layer (experimental  
23 value 0.328 nm, model value 0.338 nm) (Fig. 4(a) and model VII of table 5).  
24  
25  
26  
27  
28  
29  
30  
31  
32  
33  
34  
35  
36  
37  
38  
39  
40  
41  
42  
43  
44

45 The next stable configuration of adsorbed CO is found on  $(5 \times 2)$ -8CO with a coverage of  
46 0.8 ML. At this coverage we find three different configurations of CO on the surface that are  
47 identical in energy - CO adsorbed on (i) 6T-2B (ii) 4T-4B (iii) 2T-6B, where T represents top  
48 and quasi top site and B represents the bridge and quasi-bridge site of adsorption (structures  
49 IX, IX-a, IX-b in Table 5). When compared at 300K, the Gibbs free energy difference between  
50 these structures is less than  $2 \text{ meV}/\text{\AA}^2$ , making them computationally identical. We observe  
51  
52  
53  
54  
55  
56  
57  
58  
59  
60



that this structure is only stable at pressures above 1 Pa and temperatures above RT.

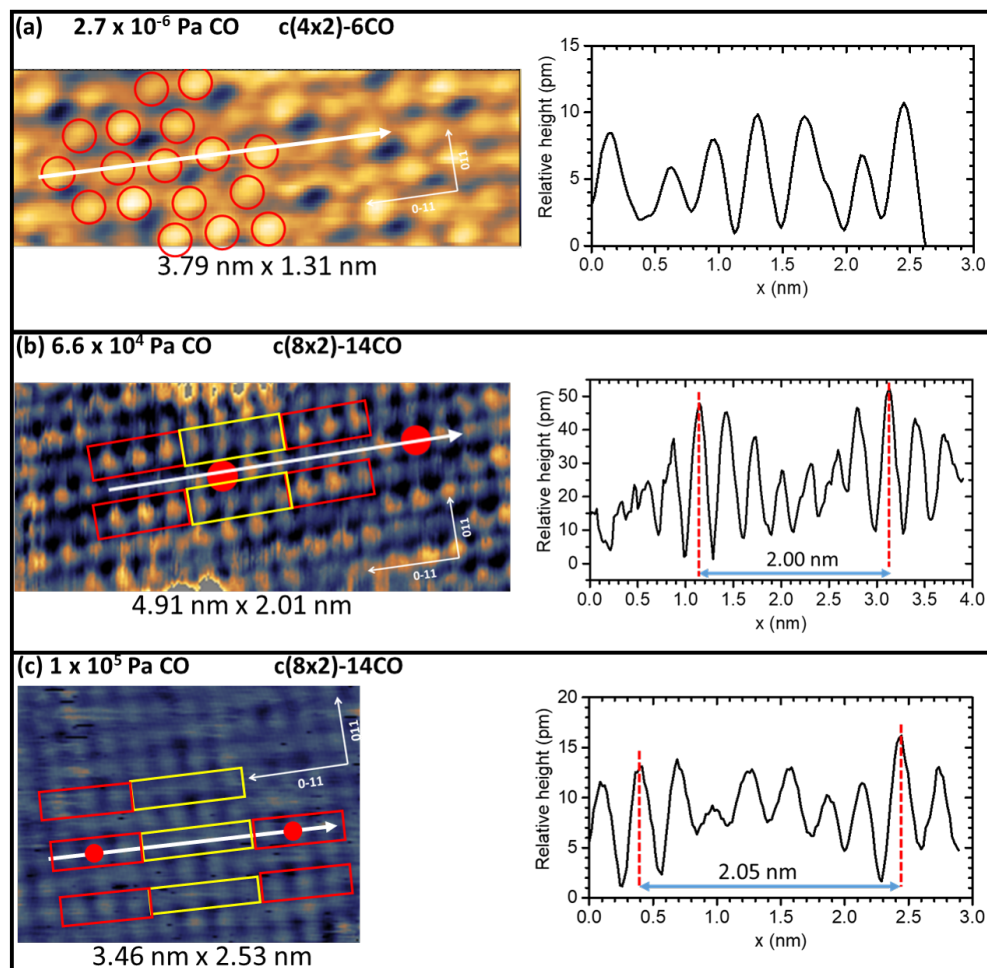


Figure 4: Over-layer structure of CO at different pressure on Pt(100) surface observed by in-situ HP-STM at room temperature. (a)  $2.7 \times 10^{-6}$  Pa CO, which indicates formation of  $c(4 \times 2)$ -6CO over-layer corresponding to  $\theta = 0.75$ . Red circles show location of adsorbed CO molecules. (b)  $6.6 \times 10^4$  Pa CO, which indicates formation of  $c(8 \times 2)$ -14CO over-layer corresponding to  $\theta = 0.875$ . (c)  $1 \times 10^5$  Pa CO. In (b) and (c), red and yellow rectangles show locations of quasi-top CO molecules and quasi-bridge CO molecules, respectively. White arrows indicate direction of scan profiles which are shown on the right side. Settings for STM acquisition are: (a) 0.50 nA, 0.60 V; (b) 1.00 nA, 0.60 V; (c) 0.85 nA, 0.90 V.

With increasing chemical potential, coverage increases and CO molecules arrange in a similar manner on a longer unit cell -  $(6 \times 2)$ -10CO, corresponding to a coverage of 0.83 ML. At this coverage, in a similar way to the  $(4 \times 2)$  unit cell case, we find that two configurations of CO molecules on the surface have similar adsorption energies - (i) 6 CO on top (and quasi-top) + 4 CO on quasi-bridge CO (ii) 4 CO on quasi-top + 6 CO bridge and quasi-bridge

(structures X and XI in table 5. The former orientation is only stable at high temperatures ( $T > 370$  K) and high pressures ( $P > 6 \times 10^4$  Pa). At the quasi-top/quasi-bridge site the adsorbed CO are tilted from the normal z-axis by a  $\pm 5.5^\circ$  angle. Such a behaviour of “fan out” helps to incorporate more adsorbate on the surface and similar observation was made previously on 2D nano-clusters on reconstructed hex-Pt(100) surface in CO environments by Tao. et. al.<sup>75</sup>.

Finally we see that the coverage saturates at 0.875 ML where two iso-energy CO configurations, (i) 8 quasi-top, 6 quasi-bridge and (ii) 6 quasi-top, 8 quasi-bridge CO adsorbed on a  $(8 \times 2)$  unit cell are stable (structures XII and XII-a in Table 5). The quasi-top adsorbed CO are tilted at an angle of  $\pm 6^\circ$  and the quasi-bridge adsorbed CO are tilted at an angle of  $\pm 5.2^\circ$  with respect to the normal z-axis.

Beyond the already discussed low pressure conditions, a high CO pressure was studied experimentally to confirm the predictions from theory (Fig. 4(b) and (c)). Two experiments were performed at rather similar near ambient pressure ( $6.6 \times 10^4$  Pa and  $10^5$  Pa). At  $6.6 \times 10^4$  Pa, they formed a  $(8 \times 2)$ -14CO over-layer structure, in agreement with the computed stability diagram (blue dots in Fig. 3). Two groups of bright protrusion in the STM can be identified (red rectangles = 3 higher protrusions, yellow rectangles = 4 lower protrusion) in Fig. 4(b) and 4(c), indicating the presence of quasi-top and quasi-bridge CO. DFT Simulated STM image of this structure (SI Fig. S11) shows brighter contrast of CO on top/quasi-top site compared to CO on bridge/quasi-bridge sites. Therefore, based on the contrast of the experimental STM image (fig. 4(b) and 4(c)), it can be deduced that configuration (i) (6 quasi-top, 8 quasi-bridge), of the two iso-energetic CO configurations mentioned earlier, is the one being observed experimentally. Interestingly, configuration (ii) (8 quasi-top, 6 quasi-bridge) was not observed in STM images.

On further examination of high coverage ( $\theta \geq 0.75$ ) structures for Pt(100), CO arranges in a skewed hexagonal matrix with average CO-CO distances smaller than that observed on Pt(111). On Pt(111), at  $\theta = 0.75$ , CO arranges on a  $p(2 \times 2)$  unit cell with CO on top, FCC and

1  
2  
3 HCP site creating a perfect hexagonal lattice with C-C distance of 3.25 Å. In comparison,  
4 for Pt(100), the average C-C distance for CO on (4x2), (6x2) and (8x2) is 3.22 (2.22%  
5 smaller), 3.18 (3.4%) and 2.93 (11.02%) respectively. The superimposed distorted hexagonal  
6 configuration of CO on Pt(100) reduces the repulsion between adjacent CO molecules and  
7 therefore decreases the energy. Hence for a given condition (for example standard condition  
8 at room temperature) the density of chemisorbed CO molecules is larger on Pt(100) (0.11 in  
9 CO/Å<sup>2</sup>) than on Pt(111) (0.099 in CO/Å<sup>2</sup>). This is due to the lower Pt-Pt coordination on  
10 Pt(100) resulting in a larger CO adsorption energy, that is able to compensate a stronger CO-  
11 CO repulsion energy and lead to a larger CO density at equilibrium. It's worth highlighting  
12 that using the generalized correction,  $\Delta = 4.77d_{CO} - 5.37$  eV, results in essentially the same  
13 stability diagram (SI Fig. S11) as using the separately fitted correction terms for Pt(100)  
14 surface ( $\Delta = 4.74d_{CO} - 5.34$  eV).  
15  
16  
17  
18  
19  
20  
21  
22  
23  
24  
25  
26  
27  
28

## 29 4 Conclusion

30  
31  
32 The adsorption of CO on Pt(111) and Pt(100) was studied using an atomistic first-principles  
33 thermodynamic model and high pressure scanning tunneling microscopy. In order to correct  
34 for the site preference and for the overestimated adsorption energy, we developed a energy  
35 correction scheme based on the C-O bond distance. The magnitude of the correction is  
36 smallest for the top site, followed by the bridge and other poly-coordinated sites (threefold  
37 hcp/fcc site for Pt(111) and fourfold hollow site for Pt(100)). Using the energy correction  
38 scheme, we construct the thermodynamic stability diagram that describes the surface ter-  
39 minations as a function of temperature and pressure. The formation of dense CO layers  
40 on Pt(111) and Pt(100) follow two different modes. On Pt(111) (at  $\theta=0.25$  ML) all the  
41 adsorption sites (top, bridge, hollow) are rather equivalent in stability. In order to optimize  
42 adsorption and minimize repulsion CO molecules organize in a 2D hexagonal pattern and  
43 the adsorbate density depends on the pressure. This CO hexagonal pattern is set in registry  
44  
45  
46  
47  
48  
49  
50  
51  
52  
53  
54  
55  
56  
57  
58  
59  
60

1  
2  
3 with the surface by the coincidence of a rotated supercell of Pt(111) with a rotated supercell  
4 of the CO hexagonal lattice. From this ideal starting position, CO molecules slightly relax  
5 laterally, with also small tilts with respect to the vertical direction, and slightly deform the  
6 hexagonal pattern. A systematic computational exploration of such hexagonal coincidence  
7 structures shows that the  $(2\sqrt{3} \times 2\sqrt{3})R30^\circ$ -7CO at 0.583 ML and the  $(\sqrt{19} \times \sqrt{19})R23.4^\circ$ -  
8 13CO at 0.684 ML are the stable arrangement appearing in the calculated thermodynamic  
9 diagram. These calculated structures are in very good agreement with experimental data,  
10 as seen for example with the simulated STM image (refer figure S5 in Supporting Informa-  
11 tion). Non-hexagonal CO adlayers ( $(\sqrt{3} \times 3)$ rect-4CO and  $c(\sqrt{3} \times 7)$ rect-5CO arrangement)  
12 however appear as low energy metastable structures, explaining why in UHV at low temper-  
13 ature, these non-hexagonal layers can be observed in place of the Moiré pattern coincidence  
14 lattices.  
15  
16

17  
18  
19 On Pt(100), bridge and top sites have similar stability, but the hollow site is less stable.  
20 The CO molecules hence adopt a 1D coincidence lattice, with n-1 CO molecules placed  
21 on a dense row of n Pt atoms, with an ensemble of top sites molecules followed by an  
22 ensemble of bridge site ones. The structures relax with slight off vertical rotations on the  
23 CO molecules, illustrated as a “fan-out” movement. These “fan-out” displacements lead  
24 to reduced repulsion between CO molecules on adjacent adsorption sites. These CO rows  
25 are staggered in the perpendicular direction, forming elongated (nx2) unit cells. Our STM  
26 experiments at ambient CO pressure and room temperature on Pt(100) clearly confirm these  
27 theoretical predictions, with the formation of a highly dense (8x2)-14CO structure (coverage  
28 of 0.875 ML). These high coverage structures of CO provide structural data for the study of  
29 the catalytic reactivity and restructuring events occurring on these Pt surfaces in reactions  
30 involving high CO pressures.  
31  
32  
33  
34  
35  
36  
37  
38  
39  
40  
41  
42  
43  
44  
45  
46  
47  
48  
49  
50  
51  
52  
53  
54  
55  
56  
57  
58  
59  
60

## 4.1 Acknowledgment

This work was funded by NSF, Grant No. 1800601. This work used computational and storage services associated with the Hoffman2 Shared Cluster provided by the UCLA Institute for Digital Research and Education's Research Technology Group. The authors want to thank XSEDE (TG-CHE170060) SDSC's Comet Supercomputer and Bridges PSC for the compute time.

## References

- (1) Chorkendorff, I.; Niemantsverdriet, J. W. *Concepts of modern catalysis and kinetics*; Wiley Online Library, 2003; Vol. 138.
- (2) Allian, A. D.; Takanabe, K.; Furdala, K. L.; Hao, X.; Truex, T. J.; Cai, J.; Buda, C.; Neurock, M.; Iglesia, E. Chemisorption of CO and mechanism of CO oxidation on supported platinum nanoclusters. *Journal of the American Chemical Society* **2011**, *133*, 4498–4517.
- (3) Chua, Y. G.; Gunasooriya, G. K. K.; Saeys, M.; Seebauer, E. G. Controlling the CO oxidation rate over Pt/TiO<sub>2</sub> catalysts by defect engineering of the TiO<sub>2</sub> support. *Journal of catalysis* **2014**, *311*, 306–313.
- (4) Eichler, A. CO oxidation on transition metal surfaces: reaction rates from first principles. *Surface science* **2002**, *498*, 314–320.
- (5) Fu, Q.; Saltsburg, H.; Flytzani-Stephanopoulos, M. Active nonmetallic Au and Pt species on ceria-based water-gas shift catalysts. *Science* **2003**, *301*, 935–938.
- (6) Rodriguez, J.; Ma, S.; Liu, P.; Hrbek, J.; Evans, J.; Perez, M. Activity of CeO<sub>x</sub> and TiO<sub>x</sub> nanoparticles grown on Au (111) in the water-gas shift reaction. *Science* **2007**, *318*, 1757–1760.

- 1  
2  
3 (7) Lin, C.-H.; Chen, C.-L.; Wang, J.-H. Mechanistic studies of water–gas-shift reaction on  
4 transition metals. *The Journal of Physical Chemistry C* **2011**, *115*, 18582–18588.  
5  
6  
7  
8 (8) Grabow, L. C.; Gokhale, A. A.; Evans, S. T.; Dumesic, J. A.; Mavrikakis, M. Mechanism  
9 of the water gas shift reaction on Pt: First principles, experiments, and microkinetic  
10 modeling. *The Journal of Physical Chemistry C* **2008**, *112*, 4608–4617.  
11  
12  
13  
14 (9) Dry, M. E. The fischer–tropsch process: 1950–2000. *Catalysis today* **2002**, *71*, 227–241.  
15  
16  
17  
18 (10) Khodakov, A. Y.; Chu, W.; Fongarland, P. Advances in the development of novel  
19 cobalt Fischer- Tropsch catalysts for synthesis of long-chain hydrocarbons and clean  
20 fuels. *Chemical reviews* **2007**, *107*, 1692–1744.  
21  
22  
23  
24 (11) Den Breejen, J.; Radstake, P.; Bezemer, G.; Bitter, J.; Frøseth, V.; Holmen, A.;  
25 De Jong, K. On the origin of the cobalt particle size effects in Fischer- Tropsch catalysis.  
26 *Journal of the American Chemical Society* **2009**, *131*, 7197–7203.  
27  
28  
29  
30  
31 (12) Somorjai, G. A.; Li, Y. *Introduction to surface chemistry and catalysis*; John Wiley &  
32 Sons, 2010.  
33  
34  
35  
36 (13) Avery, N. R. Electron energy loss spectroscopic study of CO on Pt (111). *The Journal*  
37 *of chemical physics* **1981**, *74*, 4202–4203.  
38  
39  
40  
41 (14) Shigeishi, R.; King, D. A. Chemisorption of carbon monoxide on platinum {111}:  
42 Reflection-absorption infrared spectroscopy. *Surface Science* **1976**, *58*, 379–396.  
43  
44  
45  
46 (15) Crossley, A.; King, D. A. Infrared spectra for co isotopes chemisorbed on Pt “111”:  
47 Evidence for strong adsorbate coupling interactions. *Surface Science* **1977**, *68*, 528–  
48 538.  
49  
50  
51  
52 (16) Ertl, G.; Neumann, M.; Streit, K. Chemisorption of CO on the Pt (111) surface. *Surface*  
53 *Science* **1977**, *64*, 393–410.  
54  
55  
56  
57  
58  
59  
60

- 1  
2  
3 (17) Hopster, H.; Ibach, H. Adsorption of CO on Pt (111) and Pt 6 (111)×(111) studied by  
4 high resolution electron energy loss spectroscopy and thermal desorption spectroscopy.  
5 *Surface Science* **1978**, *77*, 109–117.  
6  
7  
8  
9  
10 (18) Steininger, H.; Lehwald, S.; Ibach, H. On the adsorption of CO on Pt (111). *Surface*  
11 *Science* **1982**, *123*, 264–282.  
12  
13  
14 (19) Hayden, B.; Bradshaw, A. *Studies in Surface Science and Catalysis*; Elsevier, 1983;  
15 Vol. 14; p 51.  
16  
17  
18  
19 (20) Biberrian, J.; Van Hove, M. A new model for CO ordering at high coverages on low  
20 index metal surfaces: A correlation between LEED, HREELS and IRS: II. CO adsorbed  
21 on fcc (111) and hep (0001) surfaces. *Surface science* **1984**, *138*, 361–389.  
22  
23  
24  
25 (21) Tüshaus, M.; Schweizer, E.; Hollins, P.; Bradshaw, A. Yet another vibrational study  
26 of the adsorption system Pt {111}-CO. *Journal of electron spectroscopy and related*  
27 *phenomena* **1987**, *44*, 305–316.  
28  
29  
30  
31  
32 (22) Kiskinova, M.; Szab, A.; Yates Jr, J. Compressed CO overlayers on Pt (111)—evidence  
33 for tilted CO species at high coverages by digital ESDIAD. *Surface Science* **1988**, *205*,  
34 215–229.  
35  
36  
37  
38  
39 (23) Schweizer, E.; Persson, B.; Tüshaus, M.; Hoge, D.; Bradshaw, A. The potential energy  
40 surface, vibrational phase relaxation and the order-disorder transition in the adsorption  
41 system Pt {111}-CO. *Surface Science* **1989**, *213*, 49–89.  
42  
43  
44  
45 (24) Brown, W.; Kose, R.; King, D. Femtomole adsorption calorimetry on single-crystal  
46 surfaces. *Chemical reviews* **1998**, *98*, 797–832.  
47  
48  
49  
50 (25) Lee, W.; Ford, L.; Blowers, P.; Nigg, H.; Masel, R. Why do heats of adsorption of  
51 simple gases on platinum surfaces vary so little with surface structure? *Surface science*  
52 **1998**, *416*, 141–151.  
53  
54  
55  
56  
57  
58  
59  
60

- 1  
2  
3 (26) Yang, H. J.; Minato, T.; Kawai, M.; Kim, Y. STM Investigation of CO ordering on  
4 Pt (111): From an isolated molecule to high-coverage superstructures. *The Journal of*  
5 *Physical Chemistry C* **2013**, *117*, 16429–16437.  
6  
7  
8  
9  
10 (27) McCrea, K.; Parker, J. S.; Chen, P.; Somorjai, G. Surface structure sensitivity of high-  
11 pressure CO dissociation on Pt (557), Pt (100) and Pt (111) using sum frequency  
12 generation surface vibrational spectroscopy. *Surface science* **2001**, *494*, 238–250.  
13  
14  
15  
16 (28) Norton, P.; Davies, J.; Jackman, T. Absolute coverages of CO and O on Pt (111);  
17 comparison of saturation CO coverages on Pt (100),(110) and (111) surfaces. *Surface*  
18 *Science Letters* **1982**, *122*, L593–L600.  
19  
20  
21  
22 (29) Yeo, Y.; Vattuone, L.; King, D. Energetics and kinetics of CO and NO adsorption on Pt  
23 {100}: Restructuring and lateral interactions. *The Journal of chemical physics* **1996**,  
24 *104*, 3810–3821.  
25  
26  
27  
28  
29 (30) Behm, R.; Thiel, P.; Norton, P.; Ertl, G. The interaction of CO and Pt (100). I.  
30 Mechanism of adsorption and Pt phase transition. *The Journal of Chemical Physics*  
31 **1983**, *78*, 7437–7447.  
32  
33  
34  
35 (31) Song, M.-B.; Yoshimi, K.; Ito, M. STM observations of bridge-bonded CO on Pt (111)  
36 and asymmetric on-top CO on Pt (100). *Chemical physics letters* **1996**, *263*, 585–590.  
37  
38  
39  
40 (32) Martin, R.; Gardner, P.; Bradshaw, A. The adsorbate-induced removal of the Pt {100}  
41 surface reconstruction. Part II: CO. *Surface science* **1995**, *342*, 69–84.  
42  
43  
44  
45 (33) Maniguet, S.; Mathew, R. J.; Russell, A. E. EXAFS of carbon monoxide oxidation on  
46 supported Pt fuel cell electrocatalysts. *The Journal of Physical Chemistry B* **2000**,  
47 *104*, 1998–2004.  
48  
49  
50  
51  
52 (34) Guo, N.; Fingland, B. R.; Williams, W. D.; Kispersky, V. F.; Jelic, J.; Delgass, W. N.;  
53 Ribeiro, F. H.; Meyer, R. J.; Miller, J. T. Determination of CO, H<sub>2</sub>O and H<sub>2</sub> coverage by  
54  
55  
56  
57  
58  
59  
60



- 1  
2  
3 XANES and EXAFS on Pt and Au during water gas shift reaction. *Physical Chemistry*  
4 *Chemical Physics* **2010**, *12*, 5678–5693.  
5  
6  
7  
8 (35) Lahee, A.; Toennies, J.; Wöll, C. Low energy adsorbate vibrational modes observed  
9 with inelastic helium atom scattering: CO on Pt (111). *Surface Science* **1986**, *177*,  
10 371–388.  
11  
12  
13  
14 (36) Björneholm, O.; Nilsson, A.; Tillborg, H.; Bennich, P.; Sandell, A.; Hermnäs, B.;  
15 Puglia, C.; Mårtensson, N. Overlayer structure from adsorbate and substrate core level  
16 binding energy shifts: CO, CCH<sub>3</sub> and O on Pt (111). *Surface science* **1994**, *315*, L983–  
17 L989.  
18  
19  
20  
21  
22  
23 (37) Persson, B.; Tüshaus, M.; Bradshaw, A. On the nature of dense CO adlayers. *The*  
24 *Journal of chemical physics* **1990**, *92*, 5034–5046.  
25  
26  
27  
28 (38) Longwitz, S. R.; Schnadt, J.; Vestergaard, E. K.; Vang, R. T.; Lægsgaard, E.; Stens-  
29 gaard, I.; Brune, H.; Besenbacher, F. High-coverage structures of carbon monoxide  
30 adsorbed on Pt (111) studied by high-pressure scanning tunneling microscopy. *The*  
31 *Journal of Physical Chemistry B* **2004**, *108*, 14497–14502.  
32  
33  
34  
35  
36  
37 (39) Gunasooriya, G. K. K.; Saeys, M. CO Adsorption on Pt (111): From Isolated Molecules  
38 to Ordered High-Coverage Structures. *ACS Catalysis* **2018**, *8*, 10225–10233.  
39  
40  
41  
42 (40) Bocquet, M.-L.; Sautet, P. STM and chemistry: a qualitative molecular orbital under-  
43 standing of the image of CO on a Pt surface. *Surface science* **1996**, *360*, 128–136.  
44  
45  
46  
47 (41) Kresse, G.; Gil, A.; Sautet, P. Significance of single-electron energies for the description  
48 of CO on Pt (111). *Physical Review B* **2003**, *68*, 073401.  
49  
50  
51  
52 (42) Abild-Pedersen, F.; Andersson, M. CO adsorption energies on metals with correction for  
53 high coordination adsorption sites—A density functional study. *Surface Science* **2007**,  
54 *601*, 1747–1753.  
55  
56  
57  
58  
59  
60

- 1  
2  
3 (43) Gajdoš, M.; Eichler, A.; Hafner, J. CO adsorption on close-packed transition and no-  
4 ble metal surfaces: trends from ab initio calculations. *Journal of Physics: Condensed*  
5 *Matter* **2004**, *16*, 1141.  
6  
7  
8  
9  
10 (44) Feibelman, P. J.; Hammer, B.; Nørskov, J. K.; Wagner, F.; Scheffler, M.; Stumpf, R.;  
11 Watwe, R.; Dumesic, J. The CO/Pt (111) puzzle. *The Journal of Physical Chemistry*  
12 *B* **2001**, *105*, 4018–4025.  
13  
14  
15  
16 (45) Hu, Q.-M.; Reuter, K.; Scheffler, M. Towards an exact treatment of exchange and  
17 correlation in materials: Application to the “CO adsorption puzzle” and other systems.  
18 *Physical review letters* **2007**, *98*, 176103.  
19  
20  
21  
22  
23 (46) Schimka, L.; Harl, J.; Stroppa, A.; Grüneis, A.; Marsman, M.; Mittendorfer, F.;  
24 Kresse, G. Accurate surface and adsorption energies from many-body perturbation  
25 theory. *Nature materials* **2010**, *9*, 741.  
26  
27  
28  
29  
30 (47) Gautier, S.; Steinmann, S. N.; Michel, C.; Fleurat-Lessard, P.; Sautet, P. Molecular ad-  
31 sorption at Pt (111). How accurate are DFT functionals? *Physical Chemistry Chemical*  
32 *Physics* **2015**, *17*, 28921–28930.  
33  
34  
35  
36  
37 (48) Duanmu, K.; Truhlar, D. G. Validation of density functionals for adsorption energies  
38 on transition metal surfaces. *Journal of chemical theory and computation* **2017**, *13*,  
39 835–842.  
40  
41  
42  
43 (49) Wellendorff, J.; Silbaugh, T. L.; Garcia-Pintos, D.; Nørskov, J. K.; Bligaard, T.;  
44 Studt, F.; Campbell, C. T. A benchmark database for adsorption bond energies to  
45 transition metal surfaces and comparison to selected DFT functionals. *Surface Science*  
46 **2015**, *640*, 36–44.  
47  
48  
49  
50  
51  
52 (50) Wang, Y.; de Gironcoli, S.; Hush, N. S.; Reimers, J. R. Successful a priori modeling of  
53 CO adsorption on pt (111) using periodic hybrid density functional theory. *Journal of*  
54 *the American Chemical Society* **2007**, *129*, 10402–10407.  
55  
56  
57  
58

- 1  
2  
3 (51) Doll, K. CO adsorption on the Pt (1 1 1) surface: a comparison of a gradient corrected  
4 functional and a hybrid functional. *Surface science* **2004**, *573*, 464–473.  
5  
6  
7  
8 (52) Blyholder, G. Molecular orbital view of chemisorbed carbon monoxide. *The Journal of*  
9 *Physical Chemistry* **1964**, *68*, 2772–2777.  
10  
11  
12 (53) Hammer, B.; Morikawa, Y.; Nørskov, J. K. CO chemisorption at metal surfaces and  
13 overlayers. *Physical review letters* **1996**, *76*, 2141.  
14  
15  
16  
17 (54) Gil, A.; Clotet, A.; Ricart, J. M.; Kresse, G.; Garcia-Hernández, M.; Rösch, N.;  
18 Sautet, P. Site preference of CO chemisorbed on Pt (1 1 1) from density functional  
19 calculations. *Surface science* **2003**, *530*, 71–87.  
20  
21  
22  
23 (55) Mason, S. E.; Grinberg, I.; Rappe, A. M. First-principles extrapolation method for ac-  
24 curate CO adsorption energies on metal surfaces. *Physical Review B* **2004**, *69*, 161401.  
25  
26  
27  
28 (56) Van Santen, R. A.; Neurock, M. *Molecular heterogeneous catalysis: a conceptual and*  
29 *computational approach*; John Wiley & Sons, 2009.  
30  
31  
32  
33 (57) Held, G.; Schuler, J.; Sklarek, W.; Steinrück, H.-P. Determination of adsorption sites  
34 of pure and coadsorbed CO on Ni (111) by high resolution X-ray photoelectron spec-  
35 troscopy. *Surface science* **1998**, *398*, 154–171.  
36  
37  
38  
39 (58) Talbi, D.; Chandler, G. Extensive ab Initio Study of the C<sub>2</sub>O<sub>2</sub>, C<sub>2</sub>S<sub>2</sub>, and C<sub>2</sub>OS Sys-  
40 tems: Stabilities and Singlet- Triplet Energy Gaps. *The Journal of Physical Chemistry*  
41 *A* **2000**, *104*, 5872–5881.  
42  
43  
44  
45 (59) Tao, F.; Nguyen, L.; Zhang, S. Design of a new reactor-like high temperature near am-  
46 bient pressure scanning tunneling microscope for catalysis studies. *Review of Scientific*  
47 *Instruments* **2013**, *84*, 034101.  
48  
49  
50  
51  
52  
53 (60) Koper, M. T.; van Santen, R. A.; Wasileski, S. A.; Weaver, M. J. Field-dependent  
54 chemisorption of carbon monoxide and nitric oxide on platinum-group (111) surfaces:  
55  
56  
57  
58  
59  
60

- 1  
2  
3 Quantum chemical calculations compared with infrared spectroscopy at electrochemical  
4 and vacuum-based interfaces. *The Journal of Chemical Physics* **2000**, *113*, 4392–4407.  
5  
6  
7
- 8 (61) Illas, F.; Zurita, S.; Rubio, J.; Marquez, A. Origin of the vibrational shift of CO  
9 chemisorbed on Pt (111). *Physical Review B* **1995**, *52*, 12372.  
10  
11  
12
- 13 (62) Yeo, Y.; Vattuone, L.; King, D. Calorimetric heats for CO and oxygen adsorption and  
14 for the catalytic CO oxidation reaction on Pt {111}. *The Journal of chemical physics*  
15 **1997**, *106*, 392–401.  
16  
17  
18
- 19 (63) Tao, F.; Crozier, P. A. Atomic-scale observations of catalyst structures under reaction  
20 conditions and during catalysis. *Chemical reviews* **2016**, *116*, 3487–3539.  
21  
22  
23
- 24 (64) Teschner, D.; Révay, Z.; Borsodi, J.; Hävecker, M.; Knop-Gericke, A.; Schlögl, R.; Mil-  
25 roy, D.; Jackson, S. D.; Torres, D.; Sautet, P. Understanding palladium hydrogenation  
26 catalysts: when the nature of the reactive molecule controls the nature of the catalyst  
27 active phase. *Angewandte Chemie International Edition* **2008**, *47*, 9274–9278.  
28  
29  
30  
31  
32
- 33 (65) Reuter, K.; Scheffler, M. Composition and structure of the RuO<sub>2</sub> (110) surface in an  
34 O<sub>2</sub> and CO environment: Implications for the catalytic formation of CO<sub>2</sub>. *Physical*  
35 *Review B* **2003**, *68*, 045407.  
36  
37  
38  
39
- 40 (66) Michaelides, A.; Bocquet, M.-L.; Sautet, P.; Alavi, A.; King, D. Structures and thermo-  
41 dynamic phase transitions for oxygen and silver oxide phases on Ag {1 1 1}. *Chemical*  
42 *physics letters* **2003**, *367*, 344–350.  
43  
44  
45  
46
- 47 (67) van Spronsen, M. A.; Daunmu, K.; O'Connor, C. R.; Egle, T.; Kersell, H.; Oliver-  
48 Meseguer, J.; Salmeron, M. B.; Madix, R. J.; Sautet, P.; Friend, C. M. Dynamics of  
49 Surface Alloys: Rearrangement of Pd/Ag (111) Induced by CO and O<sub>2</sub>. *The Journal*  
50 *of Physical Chemistry C* **2018**, *123*, 8312–8323.  
51  
52  
53  
54  
55  
56  
57  
58  
59  
60

- 1  
2  
3 (68) Ogletree, D.; Van Hove, M.; Somorjai, G. LEED intensity analysis of the structures of  
4 clean Pt (111) and of CO adsorbed on Pt (111) in the c (4× 2) arrangement. *Surface*  
5 *science* **1986**, *173*, 351–365.  
6  
7  
8  
9  
10 (69) Blackman, G.; Xu, M.-L.; Ogletree, D.; Van Hove, M.; Somorjai, G. Mix of molecular  
11 adsorption sites detected for disordered CO on Pt (111) by diffuse low-energy electron  
12 diffraction. *Physical review letters* **1988**, *61*, 2352.  
13  
14  
15  
16 (70) Pedersen, M. Ø.; Bocquet, M.-L.; Sautet, P.; Lægsgaard, E.; Stensgaard, I.; Besen-  
17 bacher, F. CO on Pt (111): binding site assignment from the interplay between mea-  
18 sured and calculated STM images. *Chemical physics letters* **1999**, *299*, 403–409.  
19  
20  
21  
22 (71) Petrova, N.; Yakovkin, I. Lateral interaction and CO adlayer structures on the Pt (111)  
23 surface. *Surface science* **2002**, *519*, 90–100.  
24  
25  
26  
27 (72) Villegas, I.; Weaver, M. J. Carbon monoxide adlayer structures on platinum (111) elec-  
28 trodes: A synergy between in-situ scanning tunneling microscopy and infrared spec-  
29 troscopy. *The Journal of chemical physics* **1994**, *101*, 1648–1660.  
30  
31  
32  
33 (73) Loffreda, D.; Simon, D.; Sautet, P. Dependence of stretching frequency on surface  
34 coverage and adsorbate–adsorbate interactions: a density-functional theory approach  
35 of CO on Pd (111). *Surface science* **1999**, *425*, 68–80.  
36  
37  
38  
39 (74) Brodén, G.; Pirug, G.; Bonzel, H. Chemisorption of CO on the unreconstructed Pt  
40 (100) surface. *Surface Science* **1978**, *72*, 45–52.  
41  
42  
43  
44 (75) Tao, F.; Dag, S.; Wang, L.-W.; Liu, Z.; Butcher, D. R.; Salmeron, M.; Somorjai, G. A.  
45 Restructuring of hex-Pt (100) under CO gas environments: formation of 2-D nanoclus-  
46 ters. *Nano letters* **2009**, *9*, 2167–2171.  
47  
48  
49  
50  
51  
52  
53  
54  
55  
56  
57  
58  
59  
60

## Graphical TOC Entry

